Dispersion Interactions Between Poly(*p*–Phenylene Vinylene) Polymers

Yeo Yong Kiat

Jesus College

University of Oxford

A Thesis Submitted for the Degree of

Master in Theoretical Chemistry 2011

Department of Chemistry

Physical and Theoretical Chemistry Laboratory

Declaration of Authorship

I, Yeo Yong Kiat, hereby confirm that the work presented in this thesis is my own. Information and figures cited from other sources are given due recognition in the bibliography section.

Signature:_____ Date: _____

Contents

Acknowledgements

I would like to thank my supervisor Dr. William Barford for his guidance throughout the past four and a half months of research work. His patience through e–mails and weekly meetings has been critical in the completion of this work. I would also like to thank Nattapong Paiboonvorachat for weekly discussions in the office and over lunch, which greatly contributed to my understanding of the topic. I am also grateful to Jesada Temaismithi and Debayan Chakraborty, my fellow M.Sc. coursemates, for proofreading my thesis.

Above all, I thank God for His grace during my time at Oxford for all things and providing me with so much support through all my friends back home and in Oxford.

Abstract

Poly(*p*–phenylene Vinylene) (PPV) is an organic semiconductor that possesses many versatile electronic, optical, and mechanical properties for extensive applications and fabrication. Of particular interest is its electro–luminescence property, which is best understood in the framework of an exciton model and how PPV chains interact with one another in a solid state environment. In this work, calculation of the second–order dispersion interactions between pairs of PPV chains via perturbation theory was performed by assuming an unperturbed basis of Configuration Interaction–Singles exciton states. All calculations were made within the Pariser–Parr–Pople model and Mott–Wannier excitons were used to describe the low–lying electronic states.

The dependence of both groundstate and excited state screening energies on PPV chain length and inter–chain separation were investigated and subsequently, exploiting the pair–wise additivity of second–order dispersion interactions, screening interactions in a solid–state PPV crystal environment were estimated as well.

We find that for scaled inter–chain separations R' and number of phenylene rings N':

(1) The groundstate dispersion interaction ΔE_{GS} crosses over from a dipole–dipole interaction, where it scales as $\Delta E_{GS} \sim N^2/R^6$ for $N \ll R'$, to a line dipole–line dipole interaction, where it scales as $\Delta E_{GS} \sim N/R^5$ for $N \sim R'$.

(2) The excited state screening interaction ΔE_n crosses over from a monopole–line dipole interaction to either a dipole–dipole interaction or a line dipole–line dipole interaction when R exceeds a certain limit R_c, which can be associated

with the root–mean–square value of the exciton's relative coordinate r_{rms} (or electron–hole separation).

(3) For lattice screening, a larger value of the exciton principal quantum number n corresponds to a larger value of ΔE_n. Their magnitudes relative to the $n = 3$ exciton screening energy go as $\Delta E_{n=3} \backsimeq 2 \times \Delta E_{n=2} \backsimeq 10 \times \Delta E_{n=1}$. There is also a strong dependence of the screening energies on lattice spacing. This would mean that the screening energies would depend strongly on density fluctuations.

1 Introduction

Poly(*p*–phenylene Vinylene) (PPV) is an organic semiconductor that derives its conductivity from the π–molecular orbitals that are delocalized along its polymer backbone (molecular structure shown in Fig 1.1). Rather than its electrical properties, what launched PPV to prominence was its discovery as the first phenyl–based polymer that exhibited electroluminescence — in 1989, Burroughes *et al.* demonstrated the possibility of using PPV as an efficient emissive layer in large–area organic light emitting diodes (o–LEDs) in contrast to traditional inorganic semiconductors [1].

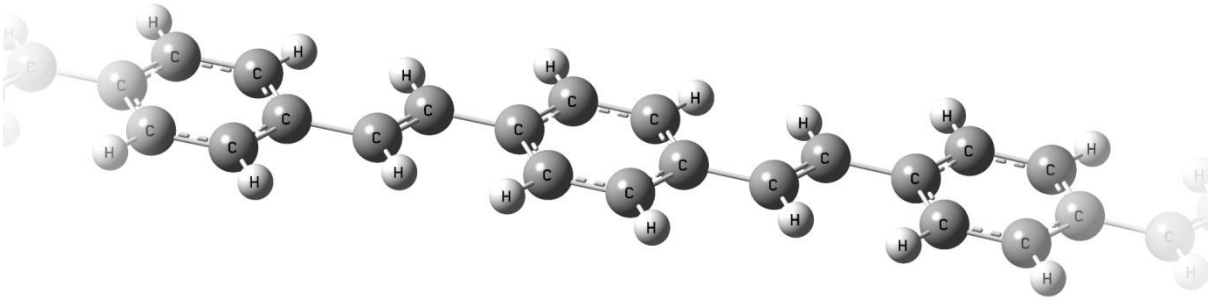

Fig. 1.1: A 3–ring segment of a PPV polymer, showing clearly the phenylene and vinylene units that make up the polymer. Each PPV chain starts and ends with a phenylene unit.

The past two decades from then have seen PPV as the subject of intense research due to certain key properties of PPV, which makes it a good choice as a model system to conduct a study:

Electronically and Optically Versatile

Undoped PPV has a very low intrinsic electrical conductivity on the order of 10^{-12} S/cm [2] — but this increases to values of 10^{-6}—10^{3} S/cm depending on the nature and concentration of the dopant, whether or not the polymer itself has been aligned by stretching or subjected to deritivatization [3]. PPV also displays strong electro– and photoluminescence in a band centred near 2.2 eV (yellow–

green light), just below the threshold for $\pi-\pi^*$ interband transitions [4], yielding potential for solar cells [5].

Possibility of Derivatization

Besides doping, alkyl and phenyl side chains lower the conductivity of PPV chains while electron donating alkoxy groups increase the conductivity of PPVs doped with weak Lewis acids (i.e. I_2, BF_3). Other side chains have other effects, but two very popular alkoxy–derivatives used in PPV–based devices are MEH–PPV and MDMO–PPV (depicted in Figure 1.2). This presents huge prospects in the fine tuning of the mechanical, electronic and optical properties of PPV.

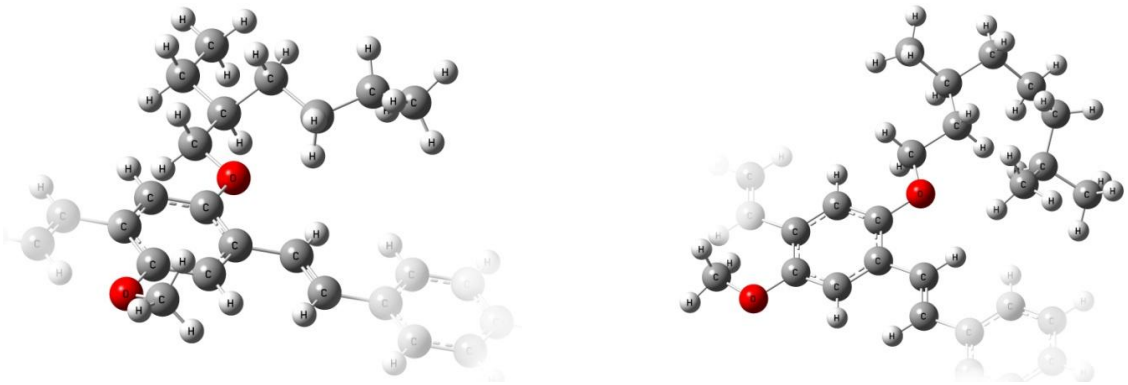

Fig. 1.2: Alkoxyl–derivatives of PPV – repeat units of MEH–PPV (left) and MDMO–PPV (right).

Ease of Fabrication

There are now various ways to synthesize thin PPV films that exhibit a high degree of crystallinity and large coherence lengths. The purity of such films prevents non–radiative decay of excited states at site defects, increasing quantum yield. One popular method is via the use of a soluble sulphonium polyelectrolyte precursor followed by a thermal conversion step [2,6] . More recently, Chemical Vapour Deposition (CVD) techniques have emerged as a lower temperature synthetic route that also allows for sequential depositions and uniform coating of irregular surfaces [7] . Coupled with its

electroluminescence property, this presents a huge potential for flat–panel display applications.

Voltaic–Tunable Electronic and Optical Properties

The electronic and optical properties of conjugated polymers such as PPV are also amenable to change when there is a voltaic stimulation to switch it between its reduced and oxidized states, which leads to a variety of potential applications [5]. These are listed in Table 1.1.

Property	Typical Change	Potential Application
Conductivity	From 10^{-7} to 10^{3} S/cm	Electronic sensors
Volume	~10%	Electromechanical actuators
Colour	300 nm shift in absorbance band	Displays, 'smart' windows
Ion Permeability	From 0 to 10^{-8} molcm^{-2}s^{-1} in solutions.	Membranes

Table 1.1: Property changes that are typically observed upon electrical stimulation to switch conjugated polymers between their reduced and oxidised states.

As with all semiconductors, the optical and electronic properties of PPV depends on the band gap, which in turn depends on how neighbouring PPV chains in the solid state interact with one another — in general, intermolecular attractions should reduce the electronic energy levels of PPV chains. Since PPV chains are charge–neutral, non–polar hydrocarbons, the primary intermolecular interaction is that of the *London dispersion* interaction.

The first quantum mechanical description of the dispersion interaction between two neutral molecules was given by London in 1930 [8] in terms of the London formula:

$$E_{disp} = -\frac{3}{2}\left(\frac{I_A I_B}{I_A + I_B}\right)\frac{\alpha_A \alpha_B}{R^6}, \qquad (4.1)$$

where I_i and α_i refer to the ionization potential and polarizability of atom i

respectively, and R is the intermolecular separation. London went on to show that this formula has the property of *additivity*, that is, if three or more molecules interact simultaneously, the three interaction potentials given by equation (1.1) can be simply added to yield the total interaction energy.

In 1937, London gave a semi–classical account of the dispersion interaction in the celebrated article *The General Theory of Molecular Forces* [9]. He presented the dispersion interaction as a *dynamic* interaction that exists between all molecules — the zero–point motion of electrons within molecules results in instantaneous dipoles that produce an instantaneous electric field to polarize neighbouring molecules to form induced dipoles.

The next 60 years saw continued corroboration of London's work; in 1962, Salem investigated the dispersion interaction between long saturated molecules by treating the σ electrons on a stand–alone basis [10]. By integrating equation (2.1) over a line, he discovered that when the chain length L is much greater than R, the dispersion energy scaled as $E_{disp} \sim L/D^5$, and when $R \gg L$, it scaled as $E_{disp} \sim L^2/D^6$.

More modern treatments of the dispersion interaction have emerged and in a series of publications, Becke and Johnson [11] have suggested that the instantaneous dipole moments be represented as *position–dependent* dipole moments, which can be associated with electrons and their *exchange–holes*, which accompanies the electrons as they move. This model has already been extended to higher–order dispersion coefficients by generalizing the treatment from dipoles to quadrupoles and octupoles. The same scaling laws were obtained in this study as well.

More relevant to this work is the recent work by Barford and Xu [12] where they applied a model of Mott–Wannier excitons and perturbation theory to determine

the groundstate screening energies of conjugated polymers. Although it was an approximate method based on the Pariser–Parr–Pople model [13], it allowed for data for systems of longer chains to be obtained. It was found that the dispersion energy scaled as $E_{disp} \sim L/R^5$ when $R \gg L$, and scaled as $E_{disp} \sim L^2/R^6$ when $R \gg L$.

To explain their results, the *distributed–dipole model* was used [14,15]. Very briefly, it describes the electronic fluctuations in a conjugated polymer in terms of '*sub–dipoles*' localized on each repeat unit. These 'sub–dipoles' generate a longitudinal electric field that polarizes neighbouring chains, creating 'sub–dipoles' on each unit as well. It is the interaction between these two sets of 'sub–dipoles' that results in the dispersion interaction. When $R \ll L$, the chain length becomes sufficiently long for the 'sub–dipoles' along each chain to interact between themselves, giving an effective inter–chain interaction that scales as L/R^5. When $R \gg L$, the 'sub–dipoles' along different chains interact directly with a strength that scales as L^2/R^6

It is worth mentioning that much of the mathematical machinery and concepts used to describe conjugated polymers such as PPV comes primarily from solid state and condensed matter physics. The high degree of conjugation results in a valence and conduction band structure and therefore, the concept of quasi–particles is of paramount importance in understanding many physical properties of conjugated polymers. For instance, conduction of electricity along the PPV chains are actually mediated by polarons, bipolarons and even solitons — as charges are added to PPV chains, strong lattice relaxation occurs and this distortion travels along the PPV chain as the charges are carried through.

In the context of this thesis, the main quasi–particle focus is placed on low–lying exciton states and the aim of this project is to calculate the second–order

dispersion interactions between pairs of PPV chains via perturbation theory by assuming an unperturbed basis of Configuration Interaction–Singles exciton states. All calculations are made within the Pariser–Parr–Pople model. This forms an extension of the work that has already been done by Barford *et al.* with poly(acetylene) and poly(*p*–phenylene) polymers [16].

In very straightforward terms, an exciton is an electrically neutral quasi–particle that corresponds to a bound electron–hole pair, held by the Coulombic interaction. When a photon is absorbed by a PPV chain, it excites an electron from the valence band into the conduction band, creating a hole in the valence band. The Coulombic attraction between the negatively charged electron and positively charged hole results in a state that is more stable than the unbound electron–hole pair.

Some excitons have *hydrogenic* wave functions — however, the binding energy is much smaller and the size is much larger than that of a hydrogen atom because there exists screening interactions between the electron and the hole from other electrons in the solid state environment. These two parameters are useful in classifying the type of excitons in semiconductors:

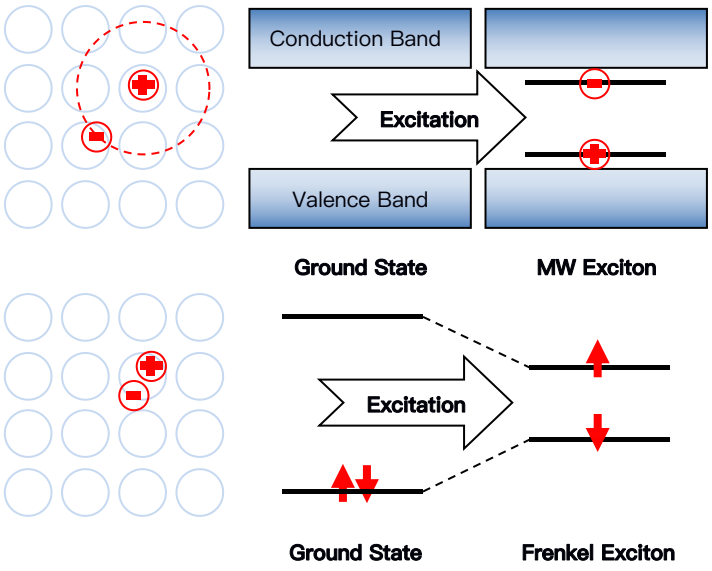

Fig. 1.3: Schematic illustrations of Mott–Wannier and Frenkel excitons in terms of lattice localization and electronic structure.

Inorganic semiconductors have strong intersite coupling interactions, resulting in larger dielectric constants and larger screening effects — this results in a smaller binding energy (~0.1 eV) and a larger exciton radius compared to the lattice spacing. Excitons in this limit are called *Mott–Wannier excitons* [17,18], where the Coulombic interaction is small compared to the bandwidth. Here, the electronic excitation is delocalized in valence and conduction bands.

Organic semiconductors have smaller dielectric constants and exhibit smaller screening effects — larger binding energies (~1 eV) and a smaller exciton radius result consequently. Excitons in this limit are called *Frenkel excitons* [19]. Here, the electronic excitation is delocalized due to intermolecular coupling and there is strong configurational mixing between molecular states.

There has been a long debate as to whether conjugated polymers are closer to organic or inorganic solids as far as their exciton states are concerned [20,21]. The concept of exciton in conjugated polymers is somewhat complicated. If we consider a three–dimensional crystal of polymers, electronic excitations on each chain becomes mobile within the crystal as a Frenkel exciton. On the other hand, the electronic structure of each polymer chain is viewed as a one–dimensional semiconductor, hence the exciton inside each chain can be described as a Mott–Wannier exciton.

In this thesis, we will work with a Mott–Wannier exciton model within the *weak–coupling limit* where construction of the exciton basis starts from a non–interacting Hartree–Fock groundstate. Mott–Wannier excitons should be sufficient enough to describe the exciton structure within each PPV chain and the weak–coupling limit is justified because the phenylene rings in PPV chains

should allow for sufficient delocalization such that electron–electron interactions are weakened.

The following section outlines the structure of the remainder of this thesis:

Chapter 2 covers important background theory for the understanding of this work, including the Born–Oppenheimer approximation, Hartree–Fock and Configuration Interaction theories, second quantization, π–electron models used, perturbation theory and PPV geometrical parameters.

Chapter 3 gives a summary of the exciton model used in this work, based on Mott–Wannier excitons in the weak–coupling limit.

Chapter 4 presents the numerical results of this work — among which the key results being discussed are chain length and chain separation dependence of pairwise screening energies as well as lattice screening energies.

Chapter 5 is a short conclusion with a summary of the work done in this thesis.

Supplementary information may be found in the various Appendices.

2 Background Theory

In this chapter, essential concepts of electronic structure theory are introduced. The electronic problem is simplified through the Born–Oppenheimer approximation and use of Slater determinants as many–electron wave functions. It is then defined in terms of the Hartree–Fock theory and electron correlation is accounted for via the method of Configuration Interaction. Perturbation theory is also outlined as a method to calculate the dispersion interactions between PPV chains. All of the above methods are used in a second quantization framework, and there is a small section describing the use of creation and annihilation operators as well. Finally, the PPV chain geometries, crystal structure and other important parameters are given.

2.1 Electronic Structure Theory

The quantum mechanical description of the electronic structure of PPV commences with a time–independent *Schrödinger equation* of the form,

$$H_{total}\Psi_{total} = E_{total}\Psi_{total} \tag{2.1}$$

This is an eigenvalue equation of the total *Hamiltonian* operator H_{total} on a *stationary–state wave function* Ψ_{total}, which yields the corresponding energy eigenvalue E_{total}. The total Hamiltonian of a molecule containing M nuclei and N electrons, in atomic units, is

$$H_{total} = -\frac{1}{2}\sum_{i=1}^{N}\nabla_i^2 - \frac{1}{2}\sum_{A=1}^{M}\frac{\nabla_A^2}{M_A} + \sum_{i=1}^{N}\sum_{j>i}^{N}\frac{1}{r_{ij}} - \sum_{i=1}^{N}\sum_{A=1}^{M}\frac{z_A}{r_{iA}} + \sum_{A=1}^{M}\sum_{B>A}^{M}\frac{z_A z_B}{R_{AB}}, \tag{2.2}$$

where ∇^2 is the Laplace operator,

M_A is the ratio of the mass of nucleus A to the electron mass,

z_A is the nuclear charge of nucleus A,

r_{ij} is the separation between electrons i and j,

r_{iA} is the separation between electron i and nucleus A,

R_{AB} is the separation between nucleus A and B.

The electronic problem begins here, where the Schrödinger equation cannot be solved exactly if the full Hamiltonian is used. The following sections outline the successive approximations made in order to simplify and solve the equation numerically.

2.1.1 Born–Oppenheimer Approximation

The Born–Oppenheimer approximation decouples the electronic motion from the nuclear motion on the premise that the electronic motion is much faster than the nuclear motion due to their relatively smaller mass so that the electronic relaxation is instantaneous in between nuclear configurations. The electrons move in the field of fixed nuclei and at each nuclear geometry, the nuclear kinetic energies are neglected and the nuclear–nuclear repulsion becomes constant.

We can now focus solely on the electronic part of the total Hamiltonian H_{elec}, and solve the electronic Schrödinger equation with the electronic wave function Ψ_{elec} for the electronic energy E_{elec},

$$H_{elec}\Psi_{elec}(\{\mathbf{r}_i\};\{\mathbf{R}_A\}) = E_{elec}(\{\mathbf{R}_A\})\Psi_{elec}(\{\mathbf{r}_i\};\{\mathbf{R}_A\}) \tag{2.3}$$

$$H_{elec} = -\frac{1}{2}\sum_{i=1}^{N}\nabla_i^2 + \sum_{i=1}^{N}\sum_{j>i}^{N}\frac{1}{r_{ij}} - \sum_{i=1}^{N}\sum_{A=1}^{M}\frac{z_A}{r_{iA}} \tag{2.4}$$

Ψ_{elec} depends explicitly on the electronic coordinates but implicitly through the nuclear coordinates. A nuclear geometry must be specified so that the electronic Schrödinger equation can be solved at that particular geometry. The total energy at a particular geometry is obtained via,

$$E_{total} = E_{elec} + \sum_{A=1}^{M} \sum_{B>A}^{M} \frac{z_A z_B}{R_{AB}} \tag{2.5}$$

From henceforth, only the electronic Hamiltonian will be considered and will be referred to as H for simplicity. From equation (2.4), it is clear that H may be further partitioned into one– and two–electron terms,

$$H = \sum_{i=1}^{N} h(i) + \sum_{i=1}^{N} \sum_{j>i}^{N} \frac{1}{r_{ij}}, \tag{2.6}$$

where

$$h(i) = -\frac{1}{2} \sum_{i=1}^{N} \nabla_i^2 - \sum_{i=1}^{N} \sum_{A=1}^{M} \frac{z_A}{r_{iA}} \tag{2.7}$$

is a one–electron operator known as the *core–Hamiltonian operator*.

2.1.2 Many–Electron Wave Functions

The Hamiltonian in equation (2.6) does not describe electronic spin at all, and it is necessary to incorporate this electronic property into the one–electron wave functions that make up the many–electron wave functions in quantum chemistry. Such one–electron wave functions are known as *spin orbitals*, denoted as $\chi_i(\mathbf{x}_i)$:

$$\chi_i(\mathbf{x}_i) = \psi_i(\mathbf{r}_i) \cdot \alpha(\omega) \text{ or } \chi_i(\mathbf{x}_i) = \psi_i(\mathbf{r}_i) \cdot \beta(\omega), \tag{2.8}$$

$$\mathbf{x}_i = \{\mathbf{r}_i, \omega\} \tag{2.9}$$

where $\mathbf{x}_i$ is the *spin–spatial coordinate*. Each χ_i is a product of a *spatial orbital* $\psi_i(\mathbf{r}_i)$ and a spin function (either $\alpha(\omega)$ or $\beta(\omega)$), where ω is an arbitrary spin coordinate. Prior knowledge of *Dirac notation* will be assumed henceforth.

Given these spin orbitals, the simplest wave function possible is a *Hartree product*, a product of spin orbitals,

$$|\Psi_{HP}| = \prod_{i=1}^{N} \chi_i(\mathbf{x}_i) . \tag{2.10}$$

However, this wave function differentiates between electrons because it places specific electrons in specific spin orbitals (i.e. electron i in spin orbital i) and cannot satisfy the antisymmetry property with respect to the pairwise

interchange of electrons. To account for both electronic indistinguishability and wave function antisymmetry, one can take a specific linear combination of such Hartree products to form a new type of wave function known as a *Slater Determinant*,

$$|\Psi_{SD}| = \frac{1}{\sqrt{N!}} \begin{vmatrix} \chi_i(\mathbf{x}_1) & \chi_j(\mathbf{x}_1) & \cdots & \chi_k(\mathbf{x}_1) \\ \chi_i(\mathbf{x}_2) & \chi_j(\mathbf{x}_2) & \cdots & \chi_k(\mathbf{x}_2) \\ \vdots & \vdots & \ddots & \vdots \\ \chi_i(\mathbf{x}_N) & \chi_j(\mathbf{x}_N) & \cdots & \chi_k(\mathbf{x}_N) \end{vmatrix}, \tag{2.11}$$

which may be written in a short-hand notation as $|ij\ldots k|$. It satisfies the antisymmetry property because a determinant changes sign if two rows or columns are interchanged:

$$|i\ldots j\ldots k| = -|j\ldots i\ldots k|. \tag{2.12}$$

Using a Slater Determinant as a trial wave function, we can express the ground state energy of a many-electron system as,

$$E_0 = \langle\Psi_0|H|\Psi_0| = \sum_{i=1}^{N} \langle\Psi_0|h(i)|\Psi_0| + \sum_{i=1}^{N}\sum_{j>i}^{N} \langle\Psi_0|\frac{1}{r_{ij}}|\Psi_0|. \tag{2.13}$$

2.1.3 Hartree-Fock Theory

To determine the set of orbitals that yield the lowest possible energy for the Slater determinant, one first minimizes the ground state energy E_0 with respect to a set of orthonormal orbitals $\{\chi_i\}$ according to *Lagrange's method of undetermined multipliers*. There exists a set of spin orbitals known as the *canonical spin orbitals*, for which the matrix of Lagrange multipliers is diagonal and so one obtains the Hartree-Fock (HF) equation in terms of spin orbitals,

$$f(1)\chi_m(1) = \left[h(1) + \sum_n [J_n(1) - K_n(1)]\right]\chi_m(1) = \varepsilon_m\chi_m(1) \tag{2.14}$$

It is an integro-differential equation of the *Fock operator* $f(1)$ on a spin orbital, and the eigenvalue ε_m is known as the *orbital energy.* Clearly, $f(1)$ consists of

three parts; $h(1)$ was previously defined in equation (2.7), but there are two new operators:

$$J_n(1) = [\int d\mathbf{x}_2 \, \chi_n^*(2) \frac{1}{r_{12}} \chi_n(2)] \tag{2.15}$$

is a *Coulomb operator*, which represents the average local electrostatic potential at $\mathbf{x}_1$ arising from an electron in χ_n.

$K_n(1)$ is the non–local *exchange operator* and has no classical interpretation — it must be defined in terms of its action on a spin orbital,

$$K_n(1)\chi_m(1) = [\int d\mathbf{x}_2 \, \chi_n^*(2) \frac{1}{r_{12}} \chi_m(2)] \, \chi_n(1) \tag{2.16}$$

Together, they form an effective one–electron potential known as the *Hartree–Fock potential*,

$$v_{HF}(1) = \sum_n [J_n(1) - K_n(1)] \tag{2.17}$$

The orbital energy is obtained by taking the expectation value of the $f(1)$,

$$\varepsilon_m = \langle \chi_m | f | \chi_m \rangle = \langle \chi_m | h | \chi_m \rangle + \sum_n [\langle mn | mn \rangle - \langle mn | nm \rangle] \tag{2.18}$$

In practice however, a set of *spatial orbitals* $\{\psi_m\}$ are used in place of spin orbitals and equations (2.14), (2.15), (2.16) and (2.18) may be rewritten as,

$$f(1)\psi_m(1) = [h(1) + \sum_n [J_n(1) - K_n(1)]] \, \psi_m(1) = \varepsilon_m \psi_m(1) \tag{2.19}$$

$$J_n(1) = [\int d\mathbf{x}_2 \, \psi_n^*(2) \frac{1}{r_{12}} \psi_n(2)] \tag{2.20}$$

$$K_n(1)\chi_m(1) = [\int d\mathbf{x}_2 \, \psi_n^*(2) \frac{1}{r_{12}} \psi_m(2)] \, \psi_n(1) \tag{2.21}$$

$$\varepsilon_m = h_{mm} + \sum_n^{N/2} 2J_{mn} - K_{mn} \tag{2.22}$$

where

$$h_{mn} = (m|h|n) \tag{2.23}$$

$$J_{mn} = (m|J|n) \tag{2.24}$$

$$K_{mn} = (m|K|n) \tag{2.25}$$

According to the method of Roothaan [22], introducing a suitable basis set converts equation (2.14) into a set of algebraic equations known as the *Roothaan equations* that may be solved by matrix algebra. Suppose a set of K known basis functions $\{\varphi_i(\mathbf{r})\}$ are used to represent the eigenfunctions $\{\psi_m(\mathbf{r})\}$ in a linear expansion:

$$\psi_m(\mathbf{r}) = \sum_{i=1}^{K} C_{im}\,\varphi_i(\mathbf{r}) \tag{2.26}$$

This converts equation (2.14) into

$$f(1)\sum_{i=1}^{K} C_{im}\,\varphi_i(\mathbf{r}) = \varepsilon_m \sum_{i=1}^{K} C_{im}\,\varphi_i(\mathbf{r}) \tag{2.27}$$

By multiplying with $\varphi_j^*(\mathbf{r})$ on the left and then integrating over all real space, one obtains the Roothaan equations in matrix notation,

$$\sum_{i=1}^{K} C_{im}\,F_{ij} = \varepsilon_m \sum_{i=1}^{K} C_{im}\,S_{ij} \tag{2.28}$$

where

$$F_{ij} = \int \varphi_i^*(1)\,f(1)\,\varphi_j(1)\,d\mathbf{r}_1 \equiv (i|f|j) \tag{2.29}$$

$$S_{ij} = \int \varphi_i^*(1)\,\varphi_j(1)\,d\mathbf{r}_1 \equiv (i|j) \tag{2.30}$$

From here on, the problem of calculating the orbitals is reduced to a matter of determining the set of coefficients $\{C_{im}\}$ in an iterative, self–consistent manner. This is widely known in the literature as the *Self–Consistent Field* procedure and is described in Appendix A.

2.1.4 Configuration Interaction Theory

At its very core, the HF method remains a mean–field theory that neglects explicit electron–electron interactions and this implies that there will be errors in both quantitative and qualitative predictions. Moreover, HF theory is insufficient to describe the low–lying exciton states of PPV chains in general because these are two–particle objects that require at least a two–particle description. To overcome this deficiency in describing electron correlation effects,

Configuration Interaction (CI) theory is employed and this section will provide a discussion of it up to the level of CI–Singles (CI–S).

The HF method describes the PPV groundstate with the HF determinant $|\Psi_0\rangle$ that is formed by occupying the N lowest energy spin orbitals out of $2K$ orbitals obtained from the solution of the Roothaan equations. However, simple permutation tells us that ${}^{2K}C_N$ determinants may be constructed from a set of $2K$ orbitals and it is possible to use these as a basis set to expand the exact N–electron state $|\Phi_0\rangle$:

$$|\Phi_0\rangle = \psi_0|\Psi_0\rangle + \sum_{\substack{a \\ r}} \psi_a^r|\Psi_a^r\rangle + \sum_{\substack{ab \\ rs}} \psi_{ab}^{rs}|\Psi_{ab}^{rs}\rangle + \cdots, \tag{2.31}$$

where the 'ψ's are the *excitation amplitudes*, $|\Psi_a^r\rangle$ denotes a *singly–excited* determinant where spin orbital χ_a in $|\Psi_0\rangle$ has been replaced by χ_r and $|\Psi_{ab}^{rs}\rangle$ represents a *doubly–excited* determinant where χ_a and χ_b have been replaced by χ_r and χ_s, and so on.

To ease computational traction, it becomes necessary to truncate the expansion at a certain excitation level n. When the truncation is carried out at $n = 1$, only the HF groundstate and singly–excited determinants are included in the expansion and this forms the basis of CI–S:

$$|\Psi_{\mathrm{CIS}}\rangle = \psi_0|\Psi_0\rangle + \sum_{\substack{a \\ r}} \psi_a^r|\Psi_a^r\rangle \tag{2.32}$$

which satisfies the electronic Schrödinger equation as follows,

$$H|\Psi_{\mathrm{CIS}}\rangle = E_{CIS}|\Psi_{\mathrm{CIS}}\rangle \tag{2.33}$$

This equation is solved through matrix algebra, as in the HF calculation, just that a CIS expansion matrix is used instead of the molecular one. The matrix elements of the Hamiltonian need to be calculated before a diagonalization is possible. Since the orbitals were obtained via the SCF algorithm, the set of

canonical spin orbitals would have been found instead – after diagonalization, only the diagonal Fock elements are non-zero and they will be equal to the orbital energies. This allows the matrix elements to take on the general form,

$$\langle \Psi_a^r | H | \Psi_b^s | = (E_0 + \varepsilon_r - \varepsilon_a)\delta_{ab}\delta_{rs} - \langle rb||sa| \tag{2.34}$$

where δ_{ij} is equal to 1, if $i = j$, and 0, if otherwise (*Kronecker's delta*),
$E_0 = \sum_a \langle a|h|a| + \frac{1}{2}\sum_a \sum_{b \neq a} \langle ab||ab|$ is the groundstate energy.

In practice, the evaluation of the matrix elements is performed with a *spin-adapted basis*, where the basis states are eigenstates of the *total spin operator* and can thus be directly related to physical states. For a single excitation, such configurations are defined as,

Singlet Configuration:
$$/ {}^1\Psi_a^r| = \frac{1}{\sqrt{2}}(/\Psi_{\bar{a}}^{\bar{r}}| + /\Psi_a^r|) \tag{2.35}$$

Triplet Configuration:
$$/ {}^3\Psi_a^r| = \frac{1}{\sqrt{2}}(/\Psi_{\bar{a}}^{\bar{r}}| - /\Psi_a^r|) \tag{2.36}$$

The matrix elements within the space of these spin-adapted configurations may now be written as,

$$\langle {}^1\Psi_a^r|H| {}^1\Psi_a^r| = (E_0 + \varepsilon_r - \varepsilon_a)\delta_{ab}\delta_{rs} - (rs|ba) + 2(ra||bs) \tag{2.37}$$
$$\langle {}^3\Psi_a^r|H| {}^3\Psi_a^r| = (E_0 + \varepsilon_r - \varepsilon_a)\delta_{ab}\delta_{rs} - (rs|ba) \tag{2.38}$$
$$\langle {}^1\Psi_a^r|H| {}^3\Psi_a^r| = 0 \tag{2.39}$$

Although the main drawbacks of the CI method include the lack of size consistency and a poor scaling with the number of electrons in the system, it has the advantage of being a variational method and does provide an exact solution to the electronic Hamiltonian within the space spanned by the basis set used. In the context of this work, the two-particle exciton states fit naturally into the two-particle framework of CI-S.

2.2 Second Quantization

The second quantization framework is a mathematical formalism that transfers the antisymmetry property of many–electron wave functions onto the algebraic properties of operators known as *creation* and *annihilation* operators [23]. A brief outline of how it is applied to fermionic systems is given in this section.

2.2.1 Creation and Annihilation Operators

A *creation* operator $c_i^\dagger$ is defined by its action on a spin orbital χ_i as

$$c_i^\dagger |k\ldots l\rangle = |ik\ldots l\rangle, \tag{2.40}$$

where $|k\ldots l\rangle$ is a general Slater determinant. It creates an electron that is placed as the first index to the left.

The anticommutation relation for the *creation* operator is given as,

$$\{c_i^\dagger, c_j^\dagger\} = c_i^\dagger c_j^\dagger + c_j^\dagger c_i^\dagger = 0. \tag{2.41}$$

For $i = j$, we have:

$$c_i^\dagger c_i^\dagger = -c_i^\dagger c_i^\dagger = 0. \tag{2.42}$$

This illustrates the Pauli principle, where no two electrons may occupy the same spin orbital. More generally,

$$c_i^\dagger |k\ldots l\rangle = 0 \quad \text{if } i \in \{k, \ldots, l\}. \tag{2.43}$$

The *annhilation* operator c_i is the adjoint of $c_i^\dagger$ and similarly, is defined by its action on a spin orbital χ_i as

$$c_i |ik\ldots l\rangle = |k\ldots l\rangle, \tag{2.44}$$

where it only destroys an electron that is placed as the first index to the left.

The anticommutation relation for c_i is obtained by taking the adjoint of equation (2.41),

$$\{c_i, c_j\} = c_i c_j + c_j c_i = 0, \tag{2.45}$$

and in general,

$$c_i|k\ldots l\rangle = 0 \quad \text{if } i \notin \{k, \ldots, l\}, \tag{2.46}$$

which means that you cannot remove an electron from a spin orbital if the spin orbital is not occupied in the first place.

There is also an anticommutation relation that relates both c_i and $c_j^\dagger$,

$$\{c_i, c_j^\dagger\} = c_i c_j^\dagger + c_j^\dagger c_i = \delta_{ij}. \tag{2.47}$$

The antisymmetry of the many–electron wave function is totally contained in all three anticommutation relations.

2.2.2 The Vacuum State

A *vacuum* state, $|0\rangle$, is defined as a state that contains no electrons at all. It is a normalized state,

$$\langle 0|0\rangle = 1 \tag{2.48}$$

This definition allows a second quantization definition of Slater determinants in general,

$$c_i^\dagger c_j^\dagger \ldots c_k^\dagger |0\rangle = |ij\ldots k\rangle. \tag{2.49}$$

Because no spin orbitals are occupied at all, we have,

$$c_i|0\rangle = 0 \tag{2.50}$$

2.2.3 Excited Determinants and the Electronic Hamiltonian

In Configuration Interaction theory, the excited determinants have a second–quantization definition as well,

$$\langle \Psi_a^r | \equiv c_r^\dagger c_a | \Psi_0 \rangle, \quad \langle \Psi_{ab}^{rs} | \equiv c_r^\dagger c_s^\dagger c_b c_a | \Psi_0 \rangle, \quad \text{etc.} \tag{2.51}$$

The electronic Hamiltonian now also has a second quantization definition in terms of the matrix elements,

$$H = O_1 + O_2 \tag{2.52}$$

$$O_1 = \sum_{i,j} \langle i | h | j \rangle c_i^\dagger c_j, \; O_2 = \frac{1}{2} \sum_{i,j,k,l} \langle ij | k l \rangle c_i^\dagger c_j^\dagger c_l c_k . \tag{2.53}$$

2.3 π–Electron Models

It is possible to show that the σ–electrons may be decoupled from the π–electrons so that we may focus solely on the latter to describe the low–energy physics of PPV chains [21]. However, even the complete π–electron–nuclear Hamiltonian remains much too complicated for an exact solution. The solution is to then turn towards idealized π–electron models to simplify the mathematics and capture the essential physics. The accuracy of these models are then further improved by using semi–empirical parameters to fit the calculations according to some known experimental results. The π–electron models used in this work are described in this section.

2.3.1 The Hückel Model

In the SCF algorithm outlined in Appendix A, the first step was to construct a trial density matrix by guessing an initial π–Hamiltonian matrix. A good initial guess would be the Hückel model Hamiltonian, which assumes static nuclear positions and neglects all electron–electron interactions. It was first proposed by Erich Hückel in 1930 [24] for the determination of molecular orbital energies in conjugated hydrocarbon systems and is defined in the context of second quantization as

$$H_\pi^{\text{Hückel}} = -\sum_{i,j} \sum_\sigma t_{ij} \left(c_{i\sigma}^\dagger c_{j\sigma} + c_{j\sigma}^\dagger c_{i\sigma} \right). \tag{2.54}$$

This is further simplified as follows: the value of $t_{ii} = t_i$ may be set to zero and t_{ij} is non–zero only if sites i and j are nearest–neighbours. This gives us a simplified Hückel model Hamiltonian of the form

$$H_{\pi}^{\text{Hückel}} = -\sum_{\langle i,j|}\sum_{\sigma} t_{ij}\,(c_{i\sigma}^{\dagger}c_{j\sigma} + c_{j\sigma}^{\dagger}c_{i\sigma})\,, \tag{2.55}$$

where the parentheses $\langle i,j|$ means that the sum is over all nearest–neighbour sites i and j. No two–electron integrals appear because all electron–electron interactions are neglected.

2.3.2 The Pariser–Parr–Pople Model

The Hückel model represents the limit of vanishing electron–electron interactions and the Pariser–Parr–Pople (PPP) model [13,25,26] improves the approximation by 'switching on' electron–electron interactions. In particular, it models the σ–electrons as screening the π–electron–nuclear and π–electron–π–electron interactions as follows:

1) Each π–electron experiences an effective nuclear charge per nucleus that is given by the difference between the actual nuclear charge and the number of core and σ–electrons arising from the atomic site. For PPV chains that consist only of sp^2 carbons, each atomic site has unit effective nuclear charge with one π–electron occupying a spherical p–orbital centred on each atomic site.

2) As with the Hückel model, $t_{ii} = t_i = 0$ and t_{ij} is non–zero only for nearest–neighbour sites i and j.

3) The electron–electron interaction is simplified through the Complete Neglect of Differential Overlap (CNDO) [27] assumption. When evaluating the two–electron integrals V_{ikjl}, only the diagonal terms $V_{iijj} = V_{ij}$ and $V_{iiii} =$

U are non–zero. The motivation for this is that the direct Coulomb interaction between two electrons on site i and j and two electrons on the same site i should dominate the electron–electron interactions.

4) The π –electron–nuclear and nuclear–nuclear interactions may be estimated by the interactions between the π–electrons corresponding to the same atoms because the effective nuclear charge and each π – electron have the same magnitude of charge.

With these, the PPP Hamiltonian is simply an extension of $H_{\pi}^{\text{Hückel}}$:

$$H_{\pi}^{\text{PPP}} = -\sum_{\langle i,j \rangle}\sum_{\sigma} t_{ij}\left(c_{i\sigma}^{\dagger}c_{j\sigma} + c_{j\sigma}^{\dagger}c_{i\sigma}\right)$$
$$+U\sum_{i}\left(N_{i\uparrow}-\frac{1}{2}\right)\left(N_{i\downarrow}-\frac{1}{2}\right)+\frac{1}{2}\sum_{i}\sum_{j\neq i}V_{ij}(N_i-1)(N_j-1) \qquad (2.56)$$

This is the model Hamiltonian that will be solved in this work. While V_{iiii} is identical for all sites and is parameterized by the parameter U, known as the *on–site interaction*, the two–electron integrals $\{V_{ij}\}$ representing the electron–electron interactions on separate sites are treated using the semi–empirical *Ohno potential*

$$V_{ij} = \frac{U}{\sqrt{1+(U\epsilon r_{ij}/14.397)^2}}, \qquad (2.57)$$

where ϵ is the dielectric constant and r_{ij} is the separation between electrons on site i and j, approximated by the separation between atomic site i and j. All bond lengths are in Å and all energies are in eV. This expression is an interpolation between a Coulomb potential, $e^2/4\pi\epsilon_0 r_{ij}$ as $r_{ij}\to\infty$ and an on–site Coulomb repulsion U. U may be taken to be the ionization potential minus the electron affinity, which is about 11 eV in conjugated polymers.

2.4 Perturbation Theory

The computational work in this project involves the application of time–independent Rayleigh–Schrödinger Perturbation Theory (RSPT) [28], which is an approximation technique to solve the Schrödinger equation of a system that has no analytical solution. This section gives an explanation of how RSPT is applied in the context of pairwise PPV chains.

2.4.1 Hamiltonian Set–up

Suppose we have two PPV chains described by the Hamiltonian H,

$$H = H^0 + V, \tag{2.58}$$

where H^0 is the zeroth–order Hamiltonian defined as

$$H^0 = H_1 + H_2, \tag{2.59}$$

and H_n refers to the intramolecular Hamiltonian of PPV chain n and is taken to be the PPP Hamiltonian of equation (2.56). V is the interchain Coulomb interaction operator that acts as a perturbation on H^0, having the form of

$$V = \sum_{i \in \text{Chain } 1} \sum_{j \in \text{Chain } 2} V_{ij}(N_i - 1)(N_j - 1), \tag{2.60}$$

where V_{ij} is obtained using the Ohno potential of equation (2.57).

2.4.2 Second–Order Dispersion Interactions

It is useful to exploit the particle–hole symmetry of the system by noting that for π–electron models, the expectation value of the occupancy of each site is unity such that $\langle N_i - 1| = 0$ [21]. This means that the first–order correction to the HF energy vanishes to zero. Jeziorski, Moszynski and Szalewicz have shown that the first–order correction is the electrostatic interaction between the two monomers, which should vanish to zero for two non–polar PPV chains [29]. The

leading non–zero correction term is therefore the second–order correction term, which is the dispersion interaction:

$$\Delta E_I = -\sum_{F \neq I} \frac{|V_{FI}|^2}{E_F - E_I} = -\sum_{F \neq I} \frac{|\langle F|V|I\rangle|^2}{\Delta E_1 + \Delta E_2}, \tag{2.61}$$

where $|I\rangle$ represents an unperturbed eigenstate of H^0 with energy E_I and ΔE_n is the change in energy of chain n between states $|I\rangle$ and $|F\rangle$. From henceforth, we shall distinguish between two types of dispersion interactions:

Groundstate Dispersion Interaction

This refers to the screening energy arising between two PPV chains that are simultaneously in their ground states (*cf* Fig. 2.1). The initial groundstate is simply the direct product of the groundstates of both PPV chains,

$$|I\rangle = |GS\rangle_1 \otimes |GS\rangle_2 \tag{2.62}$$

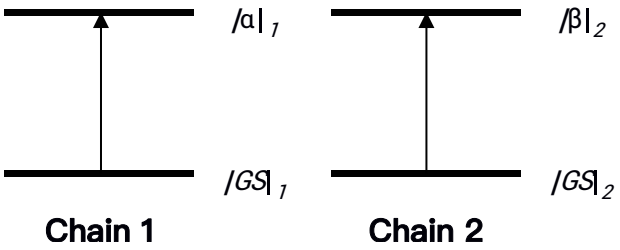

Fig. 2.1: Schematic illustration of the contributions toward the groundstate dispersion interaction

and the final excited state is the direct product of the excited states of both PPV chains,

$$|F\rangle = |\alpha\rangle_1 \otimes |\beta\rangle_2 \tag{2.63}$$

Therefore, the matrix element V_{FI} may be defined as,

$$V_{FI} = \sum_{i \in \text{Chain 1}} \sum_{j \in \text{Chain 2}} V_{ij} \left[{}_1\langle GS|N_i - 1|\alpha\rangle_1 \right] \left[{}_2\langle \beta|N_j - 1|GS\rangle_2 \right] \tag{2.64}$$

Excited State Dispersion Interaction

This refers to the screening energy arising between one chain initially in its groundstate and another initially in an excited state. There are three contributing terms to this energy (*cf* Fig. 2).

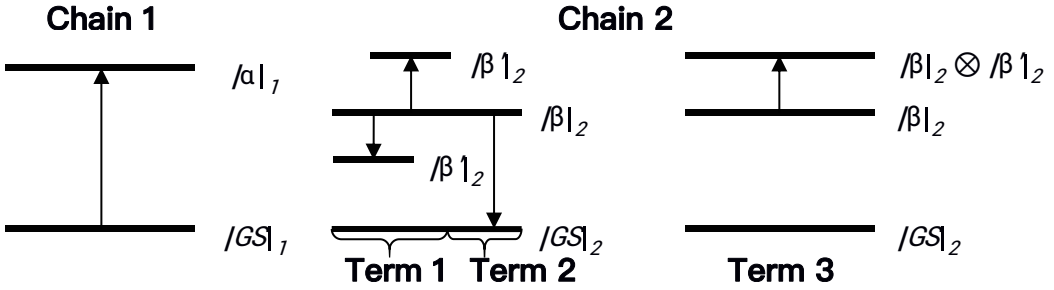

Fig. 2.2: Schematic illustration of the contributions toward the excited state dispersion interaction.

Term 1 is the dominant term that links chain 1's groundstate $|GS\rangle_1$ to an exciton state $|\alpha\rangle_1$ and chain 2's exciton state $|\beta\rangle_2$ to another exciton state $|\beta\rangle_2$ (excluding the groundstate).

The matrix element is therefore,

$$V_{FI} = \sum_{i\in\text{Chain 1}} \sum_{j\in\text{Chain 2}} V_{ij} \left[{}_1\langle GS|N_i - 1|\alpha\rangle_1 \right] \left[{}_2\langle\beta|N_j - 1|\beta\rangle_2 \right] \qquad (2.65)$$

Term 2 is smaller in magnitude, linking chain 1's groundstate $|GS\rangle_1$ to an exciton state $|\alpha\rangle_1 \neq |\beta\rangle_2$ (excluding the initial exciton state of chain 2) and chain 2's exciton state $|\beta\rangle_2$ to its groundstate $|GS\rangle_2$.

The matrix element is the same as that of equation (2.64).

Term 3 links chain 1's groundstate to an exciton state and chain 2's exciton state to a bi–exciton state. However, in the space spanned by the basis of singly–excited determinants, we may write this bi–exciton state as the direct product of two uncorrelated exciton states. Applying this approximation means that the screening interaction between the transition dipole moment of $|\beta\rangle_2$ with

that of $|\alpha|_7$ precisely negates the groundstate screening interaction between chains 1 and 2.

Therefore, Term 3 is neglected in the calculations of the screening energies.

These transition densities are derived formally in a CI–S basis in Appendix B.

2.4 PPV Crystal Structure

Since second–order dispersion interactions are pair–wise additive, a qualitative prediction for the lattice screening of the exciton states may be made by summing the screening energies of the screened chain and the screening chains. This lattice screening was calculated using the crystal structure of PPV.

The interchain packing of PPV in thin films is very regular, with a characteristic herringbone arrangement of two inequivalent chains per projected two–dimensional rectangular unit cell (*p2gg* symmetry) [30]. The Bravais lattice is monoclinic with nominal parameters $a = 8.0$Å, $b = 6.0$Å, $c = 6.6$Å (along chain axis), $\alpha = 123^{o}$ and the chain setting angle $\phi = 52^{o}$.

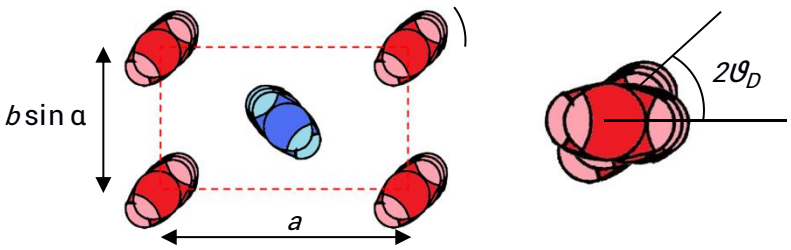

Fig. 2.3: PPV unit cell structure (left) and dihedral angle between two successive phenylene rings. Adapted from D. Chen, M. J. Winokur, M. A. Masse, and F. E. Karasz, *Polymer* **33**, 3117 (1992).

There is also significant equatorial distortion in highly oriented PPV — a non–planar thermal average chain conformation is adopted. The average dihedral angle ϑ_D formed by the plane of the phenylene ring and the vinylene unit is 8^{o} at 293 K. To calculate the dispersion energies within the crystal lattice, we

consider only nearest–neighbour and next–nearest–neighbour PPV chains in the lattice.

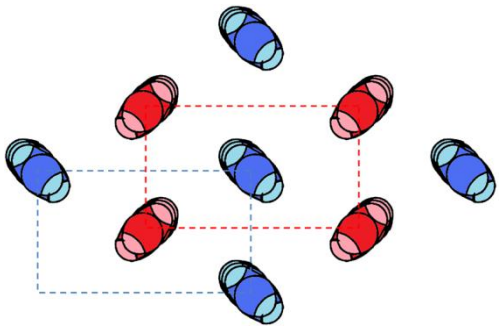

Fig. 2.4: Nearest– (red) and next–nearest–neighbour (blue) PPV chains in a PPV unit cell. The other chains in the crystal are neglected because the dispersion energies vanish rapidly with chain separation.

The screening energies between the central chain and all other chains in the manifold are then summed up to obtain the total screening energy.

2.5 PPV Geometry and Spatial Symmetry

The general PPV geometrical parameters are summarized in Fig. 2.6. The number of phenylene rings is parameterized as *N*.

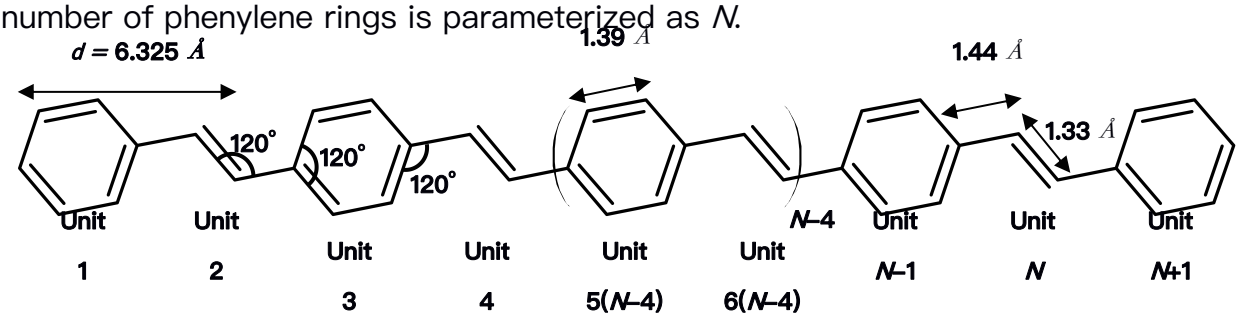

Fig. 2.5: Schematic representation of a generic PPV chain geometry.

The phenylene C=C, vinylene C=C and linking C–C bonds have bond integrals of t_p, t_d and t_s respectively. In this work, two different types of PPV chain geometries have been used in the calculation of the screening energies. Their geometries are defined in the following sections.

For convenience, the inter–chain separation is scaled by the repeat unit length d as,

$$R' = R/d \tag{2.66}$$

2.5.1 Planar PPV

This structure best represents the geometry of an isolated PPV chain *in vacuo* where electronic stability is achieved through maximizing the p_z–orbital overlap. This belongs to the point group C_{2h} and so the spatial symmetry of the molecular orbitals would be A_g and B_u for a symmetric and antisymmetric orbital respectively, with respect to a C_2 rotation about the C_2 axis, which lies perpendicular to the molecular plane through the centre of the PPV chain.

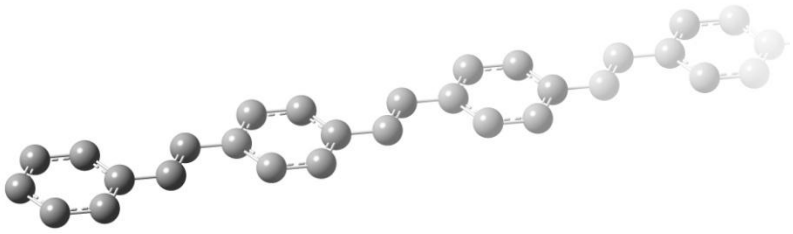

Fig 2.6: Shows the carbon skeleton of a planar PPV chain where the dihedral angle formed between the planes of the phenylene and vinylene units is zero.

2.5.2 Staggered PPV

This structure represents the geometry of a PPV chain in a solid state environment with equatorial distortion as mentioned previously. Strictly speaking, this geometry does not belong to the C_{2h} point group. However, the dihedral angle between the phenylene and vinylene units takes on a small value of only 8°. It may therefore be taken to be as good as planar so that the C_{2h} symmetry could be used to target the exciton states for convenience, as before.

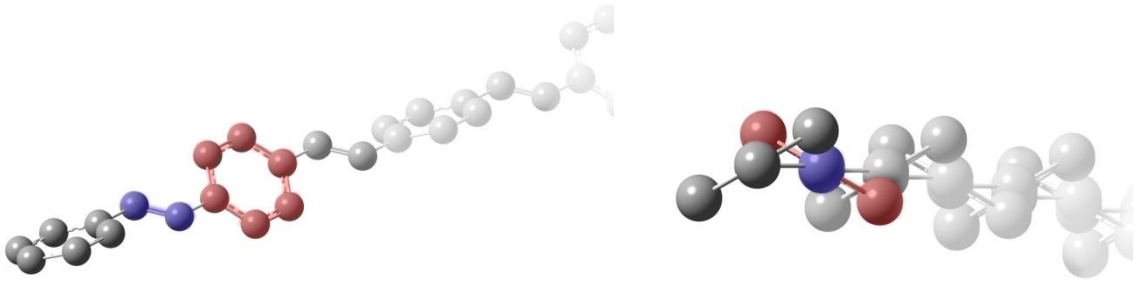

Fig 2.7: Shows the carbon skeleton of a staggered PPV chain where the dihedral angle formed between the planes of the phenylene and vinylene units alternates between 8° and -8°. The dihedral angle in this diagram has been exaggerated to 30° to illustrate the equatorial distortion more clearly.

3 The Exciton Model

As mentioned in Chapters 1 and 2, the excited states of a PPV chain are modelled as electron–hole exciton states. While the groundstate is described by the HF method, CI–S theory describes the correlation of electrons and provides an exciton basis set of singly–excited determinants to construct the exciton wave functions. This chapter will describe the Mott–Wannier exciton model and how it results from the CI–S basis.

3.1 Wannier States

For semiconductors, no doubt it would be more convenient to describe the Hamiltonian using atomic wave functions, but up till 1937, this line of approach was not adopted because atomic wave functions are not orthogonal. The use of *Bloch states* was the predominant choice until Wannier introduced the use of Wannier orbitals in 1937 [31]. Wannier orbitals are a set of orthogonal atomic wave functions that describe how each exciton is localized on a particular repeat unit of the PPV chain. It is central to the Mott–Wannier exciton model and will be introduced first.

Wannier orbitals are actually *Fourier transforms* of Bloch states. For a PPV chain that satisfies open boundary conditions, the Wannier states $|l_c^v|$ are defined as,

$$|l_c^v| = \frac{1}{\sqrt{N_u}} \sum_{\beta} |\beta_c^v| \varphi_{\beta l}^{c\,v} \tag{3.1}$$

and the corresponding creation operators are,

$$a_{l\sigma}^{c\,v\dagger} = \frac{1}{\sqrt{N_u}} \sum_{\beta} a_{\beta\sigma}^{c\,v\dagger} \varphi_{\beta l}^{c\,v} \tag{3.2}$$

where the superscripts v and c denote an orbital or electron in the *valence* and *conduction bands* respectively and $|\beta_c^v|$ is a Bloch state. Both will be introduced in Section 3.2.

In this work however, because the Wannier orbitals are localized on the repeat units of the PPV chain, we may approximate them as the molecular orbitals of the repeat unit. Two different repeat units occur along the PPV chain: ethylene units and benzene units. Their molecular orbitals are illustrated in Fig. 3.1.

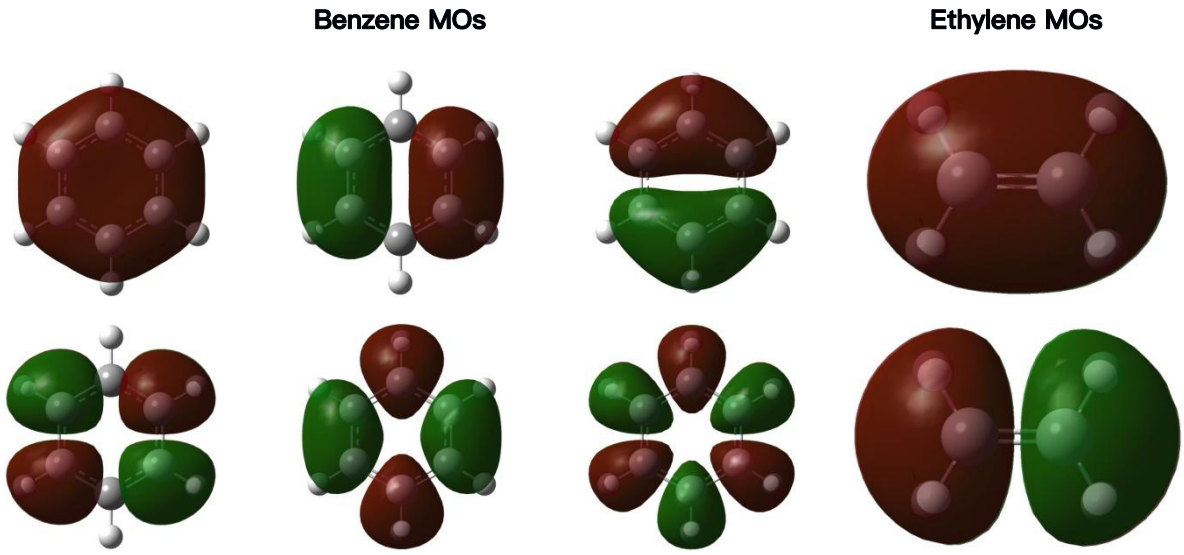

Fig. 3.1: π–Molecular orbitals of benzene and ethylene.

3.2 Valence and Conduction Bands

Previously, we have been working only in the atomic and molecular basis: while the indices $\{i\}$ referred to atomic sites, the set of indices $\{m\}$ referred to molecular orbitals. Their relation is defined by the two equations below:

$$|m\rangle = \sum_i |i\rangle C_{im} \tag{3.3}$$

$$c_m^\dagger = \sum_i c_i^\dagger C_{im} \tag{3.4}$$

where C_{im} was previously introduced in equation (2.26). However, the molecular

orbitals are better labelled as *Bloch states* – the π molecular orbitals form a lower energy, completely filled *valence band* and a higher energy, vacant *conduction band*. PPV chains possess a multi–band electronic structure, as illustrated in Fig. 3.2. Both sets of orbitals may be described by the same *pseudo Bloch wavevector* β.

If we denote the energies of the valence and conduction bands as $\{\varepsilon_\beta^v\}$ and $\{\varepsilon_\beta^c\}$ respectively, then they are related as,

$$\varepsilon_\beta^v = -\varepsilon_\beta^c. \tag{3.5}$$

Using the β notation, the HF groundstate may now be written as,

$$|\Psi_0\rangle = \prod_\beta c_{\beta\uparrow}^{v\dagger} c_{\beta\downarrow}^{v\dagger} |0\rangle \tag{3.6}$$

We now rewrite the molecular orbital coefficients C_{im} in this new β notation as well:

Valence Band MO: $C_{im} \mapsto C_{i\beta}^v,$ (3.7)

Conduction Band MO: $C_{im} \mapsto C_{i\beta}^c,$ (3.8)

such that $C_{i\beta}^v = (-1)^{i+1} C_{i\beta}^c$ (3.9)

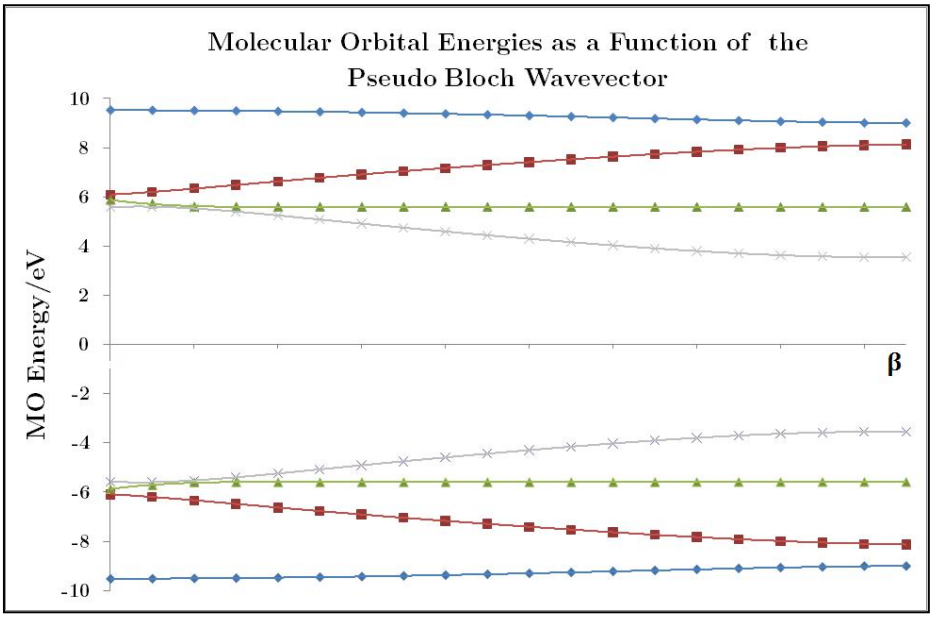

Fig. 3.2: Molecular orbital energies of a PPV chain with 20 phenylene rings. The corresponding valence–conduction bands are shown in the same colour.

3.3 Spin–Adapted States

Previously, near the end of Section 2.1.4, the concept of spin–adapted configurations was introduced. We now re–introduce them using the β notation as,

$$|{}^1_3\Psi_{ex}\rangle = \sum_{\beta_1,\beta_2} \psi^{\beta_2}_{\beta_1} |{}^1_3\Psi^{\beta_2}_{\beta_1}\rangle, \tag{3.10}$$

where

$$|{}^1_3\Psi^{\beta_2}_{\beta_1}\rangle = \frac{1}{\sqrt{2}}\left(c^{c}_{\beta_2\uparrow} c^{v\dagger}_{\beta_1\uparrow} \pm c^{c}_{\beta_2\downarrow} c^{v\dagger}_{\beta_1\downarrow}\right)|\Psi_0\rangle \tag{3.11}$$

The right subscripts and superscripts $\{\beta_1;\beta_2\}$ in $\psi^{\beta_2}_{\beta_1}$ and $|{}^1_3\Psi^{\beta_2}_{\beta_1}\rangle$ denote the molecular orbitals in the valence and conduction band respectively while the left subscripts and superscripts '1' and '3' in $|{}^1_3\Psi^{\beta_2}_{\beta_1}\rangle$ and $|{}^1_3\Psi_{ex}\rangle$ denote a singlet and triplet state respectively. Keep in mind that these are definite eigenstates of the total spin operator.

3.4 Particle–Hole Symmetry

The PPP Hamiltonian of equation (2.56) possess *particle–hole symmetry* because it is invariant under the transformation of a particle into a hole and vice versa, by the particle–hole operator J. The action of J on the atomic creation and annihilation operators is defined as,

$$J: c_{i\sigma}^{\dagger} \longmapsto (-1)^{i} h_{i\sigma}^{\dagger} \equiv (-1)^{i} c_{i\bar{\sigma}}, \tag{3.12}$$

$$c_{i\sigma} \longmapsto (-1)^{i} h_{i\sigma} \equiv (-1)^{i} c_{i\bar{\sigma}}^{\dagger}, \tag{3.13}$$

where $h_{i\sigma}^{\dagger}$ creates a hole with spin σ, and $\bar{\sigma}$ refers to the opposite spin of σ.

Similarly, using the β notation, J may act on the molecular creation and annihilation operators as,

$$J: c_{\nu\beta\sigma}^{c\dagger} \longmapsto -c_{\beta\bar{\sigma}}^{c\nu}, \tag{3.14}$$

$$c_{\beta\sigma}^{c\nu} \longmapsto -c_{\beta\bar{\sigma}}^{c\nu\dagger}, \tag{3.15}$$

With this definition, however, the spin–adapted states of equation (3.10) are not definite eigenstates of J because,

$$J: |{}^{1}_{3}\Psi^{\beta_2}_{\beta_1}| \longmapsto \mp |{}^{1}_{3}\Psi^{\beta_1}_{\beta_2}| \tag{3.16}$$

Therefore, it is necessary to construct *particle–hole symmetry–adapted states* that are definite eigenstates of J.

3.5 Particle–Hole Symmetry–Adapted States

The particle–hole symmetry–adapted states are defined as,

Singlet:
$$|{}^{1}\Psi^{\mp}_{ex}| = \frac{1}{2}\sum_{\beta_1,\beta_2} \Psi^{\beta_2}_{\beta_1} (|{}^{1}\Psi^{\beta_2}_{\beta_1}| \pm |{}^{1}\Psi^{\beta_1}_{\beta_2}|) \tag{3.17}$$

Triplet:
$$|{}^{3}\Psi^{\pm}_{ex}| = \frac{1}{2}\sum_{\beta_1,\beta_2} \Psi^{\beta_2}_{\beta_1} (|{}^{3}\Psi^{\beta_2}_{\beta_1}| \pm |{}^{3}\Psi^{\beta_1}_{\beta_2}|) \tag{3.18}$$

From here on it becomes necessary to differentiate between particle–hole symmetry and particle–hole parity. In equations (3.17) and (3.18) above, the superscripts on the left–hand side describe the particle–hole symmetry of the state: '+' denotes an even symmetry and '—' denotes an odd symmetry. However, on the right–hand side, the positive combinations describe an even particle–hole parity, and the negative combinations describe an odd particle–hole parity.

Immediately, we see that for the same particle–hole parity, the singlet and triplet states will possess opposite particle–hole symmetries: the singlet excited states have even symmetries for odd parities and odd symmetries for even parities (the reverse is true for the triplet states).

The definition of particle–hole symmetry is given by the transformation of the particle–hole symmetry–adapted states under the action of the particle–hole exchange operator $\hat{J}$:

$$\hat{J}\,|\,{}^{1}\Psi^{\mp}_{ex}\,| \mapsto \mp\,|\,{}^{1}\Psi^{\mp}_{ex}\,| \tag{3.19}$$

$$\hat{J}\,|\,{}^{3}\Psi^{\pm}_{ex}\,| \mapsto \pm\,|\,{}^{3}\Psi^{\pm}_{ex}\,| \tag{3.20}$$

Therefore, states that are symmetric with respect to $\hat{J}$ are said to have even particle–hole symmetry and states that are antisymmetric with respect to $\hat{J}$ are of odd particle–hole symmetries.

3.6 Exciton Wave Functions

Working in the weak–coupling limit, we can describe excitons using a *real–space particle–hole basis set*. There are two parameters in this basis set: (i) R is the centre–of–mass coordinate, which represents the centre of the electron–hole pair and (ii) r is the relative coordinate, which represents the electron–hole

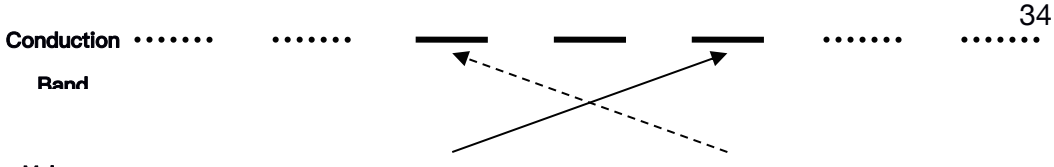

separation. The former indicates where the exciton is localized on and the latter indicates the size of the exciton.

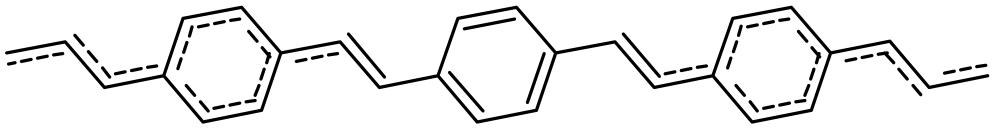

Fig. 3.2: Schematic representation of a generic PPV chain geometry.

Since the orbitals are localized on each unit of the PPV chain, we express R and r in terms of the PPV chain unit numbers, as illustrated in Fig. 3.2. We set $R = 0$ in the middle of each PPV chain.

Using Dirac notation, $|^{1}_{3}R + \frac{r}{2}, R - \frac{r}{2}|$ represents a single/triplet basis state where an electron is removed to create a hole from a valence band Wannier orbital localized at unit $R + \frac{r}{2}$ and created in a conduction band Wannier orbital localized at unit $R - \frac{r}{2}$. One can create such a state from the HF groundstate by using the basis state creation operator ${}^{1}_{3}S^{\dagger}_{Rr}$ as follows:

$$|^{1}_{3}R + \frac{r}{2}, R - \frac{r}{2}| = {}^{1}_{3}S^{\dagger}_{Rr}|\Psi_0| \tag{3.21}$$

where

$${}^{1}_{3}S^{\dagger}_{Rr} = \frac{1}{\sqrt{2}}\left(a^{c\dagger}_{R+\frac{r}{2}\downarrow} a^{v}_{R-\frac{r}{2}\downarrow} \pm a^{c\dagger}_{R+\frac{r}{2}\uparrow} a^{v}_{R-\frac{r}{2}\uparrow}\right) \tag{3.22}$$

The exciton states $|^{1}_{3}\Phi_{MW}|$ can now be expressed as linear combinations of these basis states,

$$|^{1}_{3}\Phi_{MW}| = \sum_{R,r} {}^{1}_{3}\Phi(R, r) \quad |^{1}_{3}R + \frac{r}{2}, R - \frac{r}{2}|, \tag{3.23}$$

where the coefficient of expansion ${}^{1}_{3}\Phi(R,r)$ are the exciton wave functions, which may be found by projecting $|{}^{1}_{3}\Phi_{MW}|$ onto the basis state $|{}^{1}_{3}R+\frac{r}{2},R-\frac{r}{2}|$:

$$ {}^{1}_{3}\Phi(R,r) = \langle\ {}^{1}_{3}R+\frac{r}{2},R-\frac{r}{2}|{}^{1}_{3}\Phi_{MW}| \tag{3.24} $$

$$ = \langle\Psi_0|{}^{1}_{3}S_{Rr}|{}^{1}_{3}\Phi_{MW}| \tag{3.25} $$

The exciton state $|{}^{1}_{3}\Phi_{MW}|$ can in turn be characterized by the spin–adapted and particle–hole symmetry–adapted states of equations (3.17) and (3.18) by equating $|{}^{1}_{3}\Phi_{MW}|$ to $|{}^{1}\Psi^{\mp}_{ex}|$ and $|{}^{3}\Psi^{\pm}_{ex}|$. Using variable separation, it is possible to treat the wave function as a product of two separate functions,

$$ \Phi(R,r) = \psi_n(r)\cdot\Psi_j(R) \tag{3.26} $$

The *relative wave function* $\psi_n(r)$ depends only on the relative coordinate r and is described by the *principal quantum number* n. It describes the electron–hole pair separation, giving the size of the exciton. The *centre–of–mass wave function* $\Psi_j(R)$ depends only on the centre–of–mass coordinate R and is described by the *pseudo–momentum quantum number* j. It describes the probability distribution of the location of the centre of the exciton.

3.7 Exciton Families

The exciton states can be grouped into singlet and triplet electronic states. Based on the quantum numbers n and j, it is possible to further group the exciton states into *exciton families* — for sufficiently long PPV chain lengths, the exciton energies converge to form families that are labelled with the principal quantum number n, starting from $n = 1$. Each member of a family is labelled by successively larger values of j, starting from $j = 1$.

The groundstate has the ${}^{1}A_g^+$ representation. For singlet exciton states, the $n = 1(j = 1)$ exciton state has ${}^{1}B_u^-$ symmetry and this alternates both as j increases

and as n increases. For triplet exciton states, the $n = 1 (j = 1)$ exciton state has ${}^3A_g^+$ and also alternates both as j increases and as n increases.

Unfortunately, the families form overlapping bands, such that it is difficult to identify which family an exciton state belongs to unless one examines the structure of the wave function to determine the number of nodal points. An alternative method is to turn towards the examination of exciton sizes.

3.8 Exciton Sizes

A gauge of the exciton size is given by the root–mean–square value of the relative coordinate, r_{rms},

$$r_{rms} = \sqrt{\langle r^2 |} \tag{3.27}$$

where

$$\langle r^2 | = \frac{\sum_{R,r} r^2 \Phi^2(R, r)}{\sum_{R,r} \Phi^2(R, r)} \tag{3.28}$$

In equation (3.27), $\langle r |$ is not included in the expression because $\langle r | = 0$ — due to the symmetry of $\psi_n(r)$, r has equal probability of being positive or negative. On average, an exciton with a root–mean–square value of r_{rms} may be taken to have its electron–hole separation as being r_{rms} units apart.

The r_{rms} values generally converge to finite values at infinite PPV chain lengths, with those of the same exciton family having similar sizes, as will be shown in Section 4.1.2. This provides a convenient way to determine which exciton family each exciton state belongs because there will be a discontinuous increase in the r_{rms} value if the exciton belongs to a family with a larger n value.

4 Results

This chapter will first set out to define all of the calculation parameters, such as U, ϵ, the bond integrals and $n = 3$ exciton excitation numbers. Then, using the electronic structure methods and PPV geometries described in Chapter 2, all numerical results are presented in this chapter for discussion. All data was obtained through the modification of program codes from the Barford Group at the University of Oxford, of which the codes are included in Appendix C for reference.

Pairwise screening energies were calculated for two cases: (i) having both PPV chains in the groundstate and (ii) having one PPV chain in the groundstate and another in the $n = 1$, 2 and 3 exciton state. For these calculations, planar PPV chains were used. Chain length and chain separation dependence are investigated.

Finally, lattice screening energies of the $n = 1$, 2 and 3 exciton states were also calculated, by summing up the screening of the screened chain and the other screening chains, for two cases: (i) planar PPV and (ii) staggered PPV. Chain length dependence is investigated.

4.1 Calculation Parameters

4.1.1 Semi-Empirical Parameters

The Pariser–Parr–Pople model was solved at the CI–S level using the following semi–empirical parameters for planar and staggered PPV chains:

$$U = 10.06\ eV, \quad \epsilon = 1$$
$$t_p = 2.40\ eV, \quad t_s = 2.20\ eV, \quad t_d = 2.60\ eV$$

These are '*unscreened*' parameters, which correspond to an isolated PPV chain *in vacuo* where no electrostatic screening occurs.

4.1.2 The $n = 3\ (j = 1)$ Exciton Excitation Numbers

The r_{rms} values of the exciton states were used to determine the $n = 3\ (j = 1)$ exciton excitation number — where there was a sudden increase in the r_{rms} values, it indicated a cross-over to the $n = 3$ family. Table 4.1 shows how the $n = 3\ (j = 1)$ exciton r_{rms} value steadily increases with N and eventually reaches an equilibrium value of about 5.5 units for both planar PPV and staggered PPV. It turns out that they have the exact same excitation numbers and the r_{rms} values are almost identical — this is reasonable because an equatorial distortion of 8^{o} is fairly small and planarity is mostly retained.

N	Excitation Number N_{ex}	r_{rms} (Planar)	r_{rms} (Staggered)
2*	N/A	N/A	N/A
5	9	3.577	3.576
8	13	4.756	4.752
10	16	5.113	5.105
15	24	5.419	5.410
20	31	5.494	5.483
25	39	5.520	5.510
30	46	5.533	5.522
35	54	5.539	5.528
40	61	5.543	5.532
45	69	5.545	No Calculation Performed
50	76	5.547	5.536

Table 4.1: Tabulated values of N, $n = 3$ exciton excitation numbers, N_{ex} and r_{rms} values for planar and staggered PPV (*The r_{rms} values for $N = 2$ did not exhibit a significant enough increase to accurately determine the crossover.)

There is a very high degree of linear correlation between N and N_{ex}, as Fig. 4.1 illustrates.

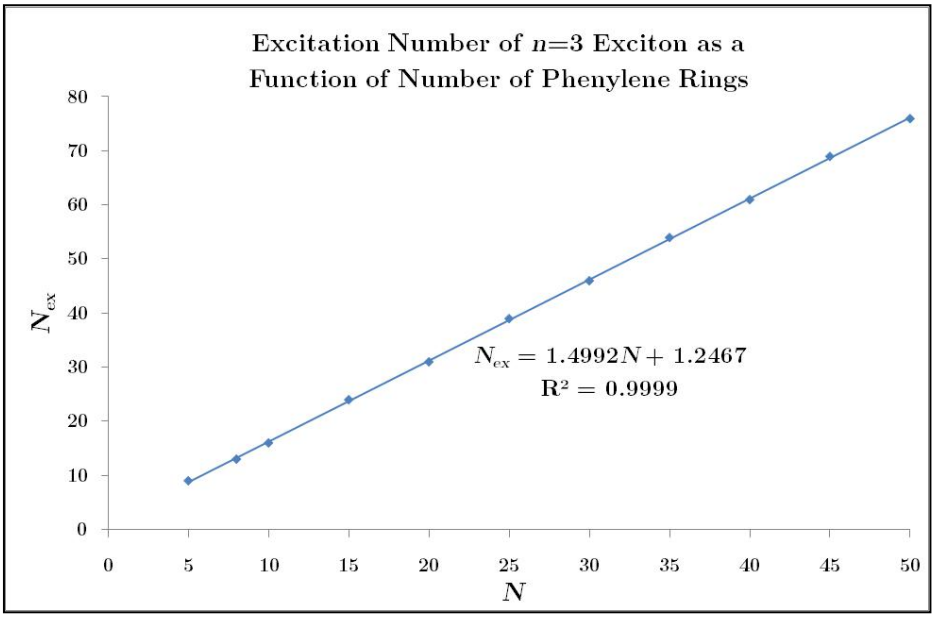

Fig. 4.1: The *n = 3* exciton excitation numbers as a function of the number of phenylene rings for planar and staggered PPV.

Using this empirical equation, it is then possible to target the *n = 3 (j = 1)* exciton state for the dispersion energy calculations for all numbers of phenylene rings in both conformations of the PPV chain.

4.2 Ground State Dispersion Interactions

4.2.1 Convergence of Ground State Dispersion Energies

Equation (2.61) for the calculation of dispersion energies involves a sum over all exciton states, but to ease computational traction, the number of such states must be truncated at some point. It is natural therefore to use the number of exciton families included in the sum as a truncation point.

Fig. 4.2 shows the ground state screening energies for a pair of parallel PPV chains plotted against the inverse of the number of exciton families retained in the sum. There is a linear convergence between the two quantities. Using the

$N = 30$ series, we find that the percentage dispersion energy recovery at the $n_{families} = 4$ and 9 limits are:

$$\frac{\Delta E_{n_{families=4}}}{\Delta E_{n_{families\to\infty}}} \% = 67\,\%, \quad \frac{\Delta E_{n_{families=9}}}{\Delta E_{n_{families\to\infty}}} \% = 85\,\%$$

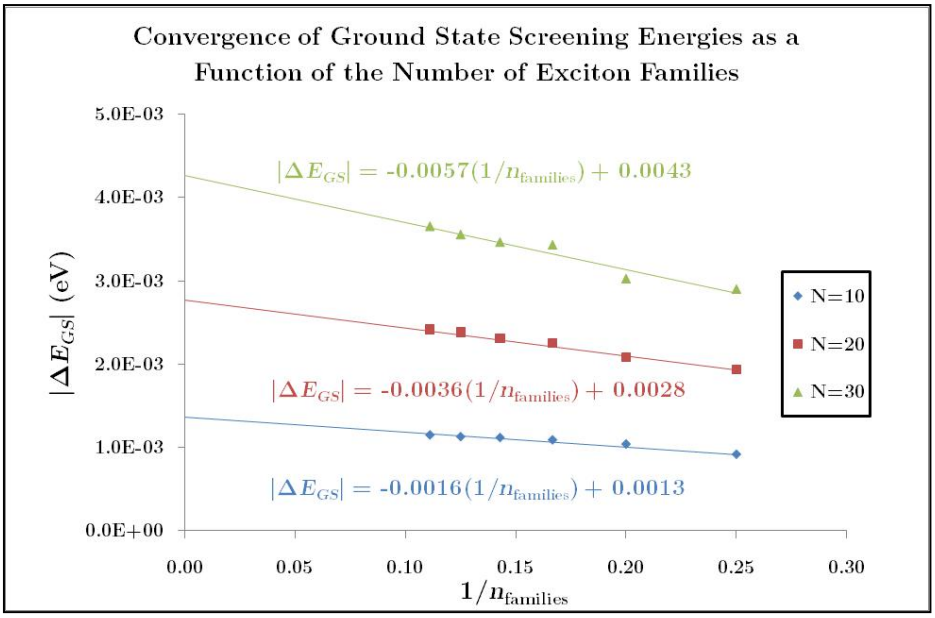

Fig. 4.2: The convergence of the ground state screening energy as a function of the number of exciton families connected to it via non–zero transition densities. The values shown above are for $N = 10 - 30$ at an inter–chain separation of $R' = 2$, where N is the number of phenylene rings, R' is the scaled inter–chain separation.

As a compromise between the accuracy of the calculation and the computational time required, all subsequent calculations were performed with retention of the first five exciton families.

4.2.2 Chain Length and Chain Separation Dependence

Fig. 4.3 shows the scaling of the pairwise groundstate screening energies as a function of the scaled inter–chain separation R', for fixed values of the number of phenylene rings N. The scaling of the groundstate dispersion interaction as a function of the number of phenylene rings, N, is shown in Fig. 4.4.

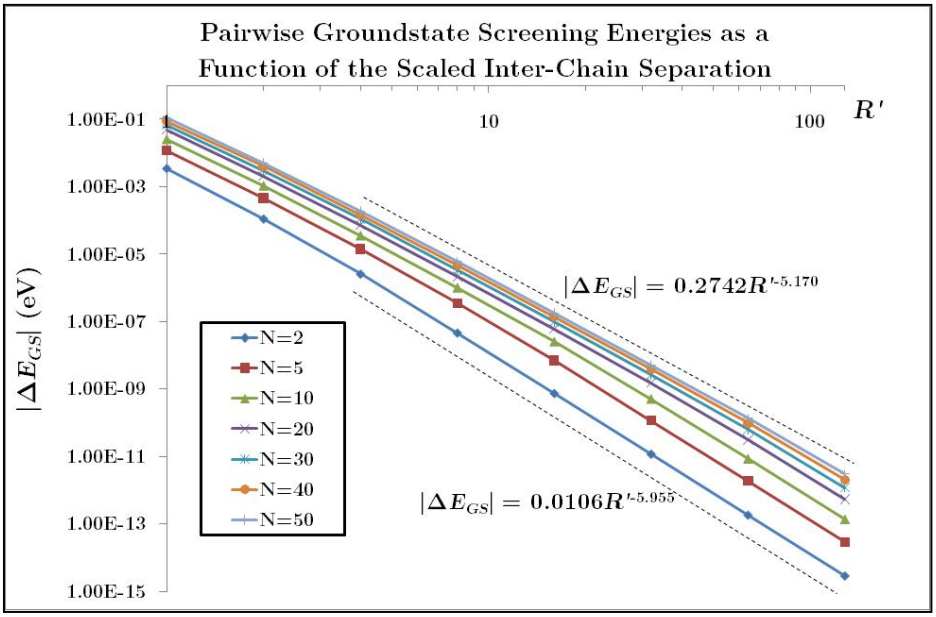

Fig. 4.3: The groundstate dispersion interaction, $|\Delta E_{GS}|$, between a pair of parallel PPV chains as a function of the scaled inter–chain separation, R'. The results show that for $N \ll R'$, $\Delta E_{GS} \sim R'^{-6}$, while for $N \sim R'$, $\Delta E_{GS} \sim R'^{-5}$. L is the length of the PPV polymer chain.

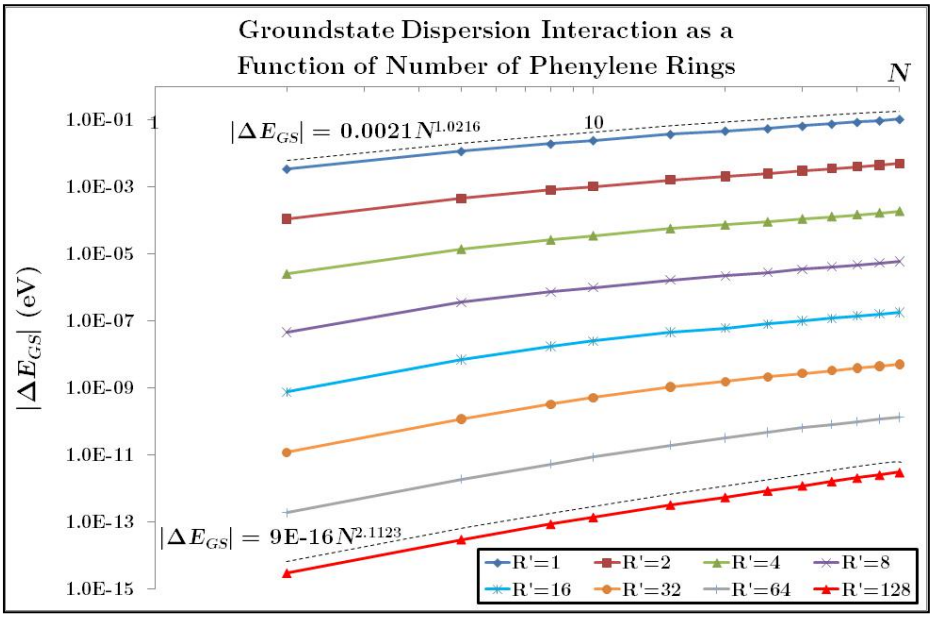

Fig. 4.4: The groundstate dispersion interaction, $|\Delta E_{GS}|$, between a pair of parallel PPV chains as a function of the number of phenylene rings, N. The results show that for $N \ll R'$, $\Delta E_{GS} \sim N^2$, while for $N \gg R'$, $\Delta E_{GS} \sim N$.

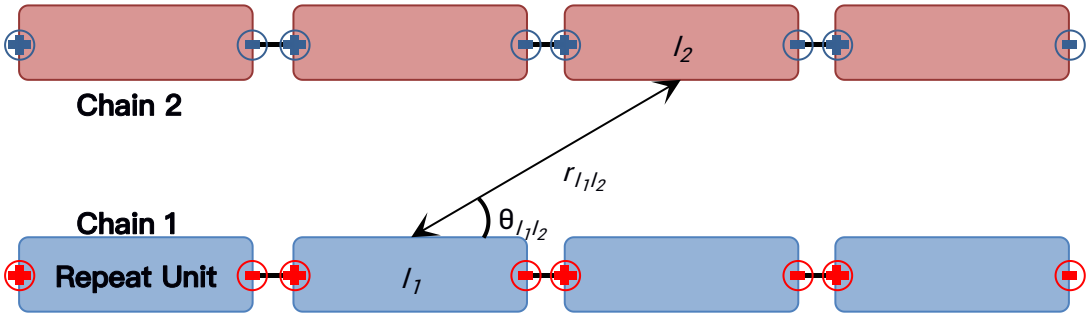

Fig. 4.5: Schematic representation of the distributed dipole approximation applied to both PPV chains in the groundstate. 'Sub–dipoles' localized on the repeat units of each chain interact between one another.

To understand the results, a brief discussion of the distributed dipole approximation mentioned in Chapter 1 will prove useful. Recall that the model assumes localized 'sub–dipoles' on each repeat unit, as shown in Fig. 4.5. Each 'sub–dipole' is a spontaneous zero–point fluctuation of the electronic motion on chain 1, which induces similar 'sub–dipoles' on chain 2. Mathematically, this is because the $|GS\rangle_1 \rightarrow |\alpha\rangle_1$ transition density alternates in sign between two sites on both chains 1 and 2. For a conjugated polymer chain of N repeat units, this semi–classical model describes the groundstate dispersion interaction ΔE_{GS} as being a sum of two terms:

$$\Delta E_{GS} = E_{GS}^{(1)} + E_{GS}^{(2)} \tag{4.1}$$

$$E_{GS}^{(1)} = -\sum_{\substack{l_1 \in \text{Chain } 1 \\ l_2 \in \text{Chain } 2}} \mu_{l_1}^{(1)} \mu_{l_2}^{(2)} \left(\frac{3\cos^2 \theta_{l_1 l_2} - 1}{4\pi\epsilon' r_{l_1 l_2}^3} \right)$$

$$= -\alpha \sum_{\substack{l_1 \in \text{Chain } 1 \\ l_1' \in \text{Chain } 1}} \mu_{l_1}^{(1)} \mu_{l_1'}^{(1)} \sum_{l_2 \in \text{Chain } 2} \frac{3\cos^2 \theta_{l_1 l_2} - 1}{4\pi\epsilon' r_{l_1 l_2}^3} \left(\frac{3\cos^2 \theta_{l_1' l_2} - 1}{4\pi\epsilon' r_{l_1 l_2}^3} \right) \tag{4.2}$$

$$E_{GS}^{(2)} = -\alpha^2 \sum_{\substack{l_2 \in \text{Chain } 2 \\ l_2' \in \text{Chain } 2}} \frac{1}{4\pi\epsilon' r_{l_1 l_2}^3}$$

$$\times \sum_{\substack{l_1 \in \text{Chain } 1 \\ l_1' \in \text{Chain } 1}} \mu_{l_1}^{(1)} \mu_{l_1'}^{(1)} \frac{3\cos^2 \theta_{l_1 l_2} - 1}{4\pi\epsilon' r_{l_1 l_2}^3} \left(\frac{3\cos^2 \theta_{l_1' l_2'} - 1}{4\pi\epsilon' r_{l_1' l_2'}^3} \right) \tag{4.3}$$

where α is the polarizability of the repeat unit, $\mu_{l_i}^{(i)}$ is the 'sub-dipole' on the l_ith repeat unit on chain i and ϵ' is the relative permittivity (dielectric constant).

$E_{GS}^{(1)}$ describes the direct interaction between the dipoles on Chain 1 and 2. $E_{GS}^{(2)}$ describes how the induced 'sub-dipoles' on Chain 2 interact between themselves to give rise to an effective interaction. In the $N \ll R'$ limit, $E_{GS}^{(1)}$ dominates and scales as N^2/R'^6. In the $N \sim R$ limit, $E_{GS}^{(2)}$ dominates and scales as N/R'^5.

The results of Fig. 4.3 and 4.4 agree with the distributed dipole approximation, and two regimes are clearly observed for inter-chain separations greater than a few lattice spacings.

1) $N \ll R'$ where $\Delta E_{GS} \sim N^2/R'^6$

The $N \ll R'$ limit refers to the limit of large inter-chain separations with respect to the chain length. This is in perfect agreement with the London formula [8] at large separations, which predicts a behaviour of $\Delta E_{GS} \sim N^2/R'^6$ for the screening energies (since chain length L is directly proportional to N). In the distributed dipole approximation, this corresponds to the *direct* dipole-dipole interaction between the 'sub-dipoles' on both PPV chains.

2) $N \sim R$ where $\Delta E_{GS} \sim N/R'^5$

The $N \sim R'$ limit refers to the limit where chain lengths become comparable to the inter-chain separations. In the distributed dipole approximation, this corresponds to an *effective* line dipole-line dipole interaction that is caused by the induced 'sub-dipoles' on Chain 2 by Chain 1 interacting between themselves — the chains become long enough for a critical number of 'sub-dipoles' to form for this interaction to dominate.

4.3 Excited State Dispersion Interactions

4.3.1 Convergence of Excited State Dispersion Energies

Fig. 4.6 shows the exciton screening energies for a pair of parallel PPV chains plotted against the inverse of the number of exciton families retained in the sum. There is a linear convergence between the two quantities — only the $n = 2$ exciton screening energies are shown for illustration. The linear fit appears to improve with a larger number of phenylene rings.

Using the $N = 30$ series, we find that the percentage dispersion energy recovery at the $n_{families} = 4$ and 9 limits are:

$$\frac{\Delta E_{n_{families}=4}}{\Delta E_{n_{families}\to\infty}} \% = 70\ \%, \quad \frac{\Delta E_{n_{families}=9}}{\Delta E_{n_{families}\to\infty}} \% = 84\ \%$$

As a compromise between the accuracy of the calculation and the computational time required, all subsequent calculations were performed with retention of the first five exciton families.

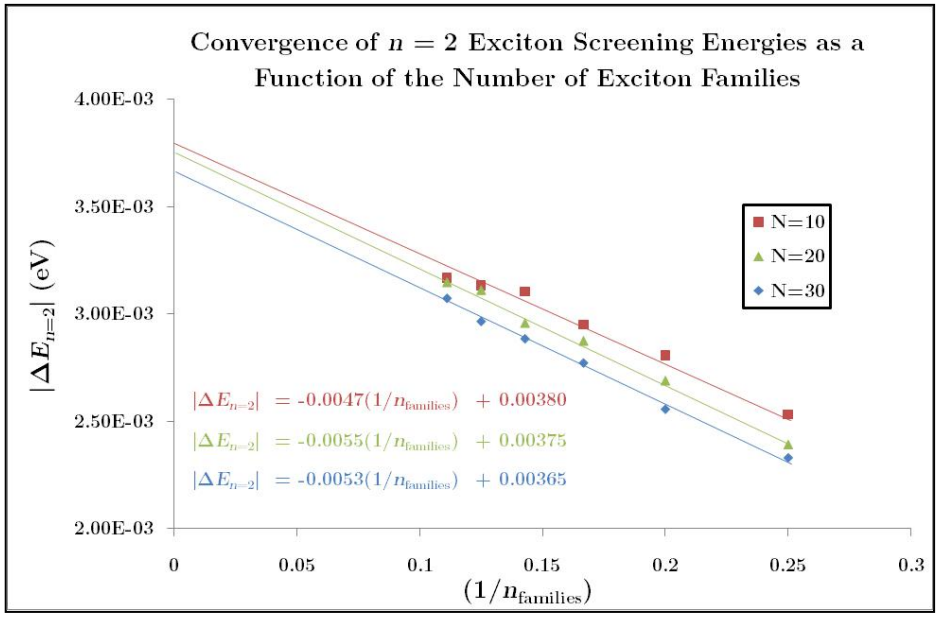

Fig. 4.6: The convergence of the $n = 2$ exciton state screening energy as a function of the number of exciton families connected to it via non-zero transition densities. The values shown above are for $N = 30$

at an inter–chain separation of $R' = 1$, where N is the number of phenylene rings, R' is the scaled inter–chain separation $R' = R/d$ and $d = 6.325\,\text{Å}$ is the repeat unit distance.

4.3.2 Chain Length and Chain Separation Dependence

Fig. 4.8 – 4.10 show the exciton screening energies for a pair of parallel PPV chains plotted against the scaled inter–chain separation while Fig. 4.11 – 4.13 show the exciton screening energies for a pair of parallel PPV chains plotted against the number of phenylene rings.

For the screening energies as a function of chain separation, for length scales greater than a lower limit, R_c, they exhibit dispersion interaction energies that scale as R'^{-6} and R'^{-5} in the exact same limits ($R_c < N \ll R'$ and $R_c < N \sim R'$ respectively) as previously described for the groundstate screening energies.

For chain separations less than R_c, we observe a crossover to a different scaling of the form $\Delta E \sim R'^{-\nu}$ where ν seems to lie between 3 and 4 (approximately 3). This crossover is not obvious for the $n = 1$ and 2 excitons because the R_c value for these two excitons is too small. The R_c value for the $n = 3$ exciton is larger and thus this crossover is much more easily observed.

The scaling of the exciton screening energies as a function of N in Fig. 4.10 – 4.12 show that for $R' \ll N$, the dispersion energy is independent of chain length (i.e. $\Delta E \sim N^0$) whereas for $N \ll R'$, the dispersion energy scales as the first power of N (i.e $\Delta E \sim N$).

We can explain these scaling laws using the distributed dipole approximation again. In the $R_c < N \ll R'$ and $R_c < N \sim R'$ limits, the dispersion interaction is a dipole–dipole and line dipole–line dipole interaction respectively, as explained earlier in Section 4.2.2. However, the crossover in the $R_c < N \sim R'$ limit (where $\Delta E \sim R'^{-\nu}$) arises due to a monopole–line dipole interaction [32,33], as illustrated in Fig. 4.7. Mathematically, the $|\beta|_2 \rightarrow |\beta|_2$ transition density does not vary in

sign between chain 2's units, which allows us to describe the charge fluctuation on chain 2 as that of monopoles.

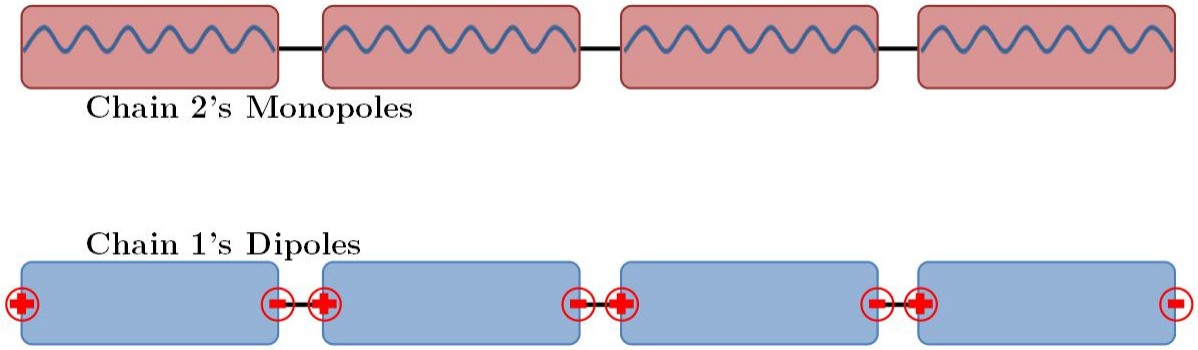

Fig. 4.7: Schematic representation of the distributed dipole approximation applied to Chain 1 in the groundstate and Chain 2 in an exciton state. 'Sub–dipoles' localized on the repeat units of Chain 1 interact with the monopoles spread out on each repeat unit of Chain 2.

What is of noteworthy interest is also how the R_c value increases from the $n = 1$ and 2 exciton value of 2 units to the $n = 3$ exciton value of 4 units. There is a correlation between the r_{rms} values of the excitons and the corresponding R_c values: while the $n = 1$ and 2 excitons possess very similar r_{rms} values of about unity, the $n = 3$ exciton possesses a larger r_{rms} value of about 5.5 units. It is therefore possible to have an approximation association of R_c with r_{rms}:

When $R' \gtrsim r_{rms}$, the dipoles on Chain 1 experience an effective dipole on Chain 2 — this leads to either a dipole–dipole or line dipole–line dipole interaction.

When $R' \lesssim r_{rms}$, the dipoles of Chain 1 experience a separate positive and negative charge on Chain 2, indicating a monopole–line dipole interaction.

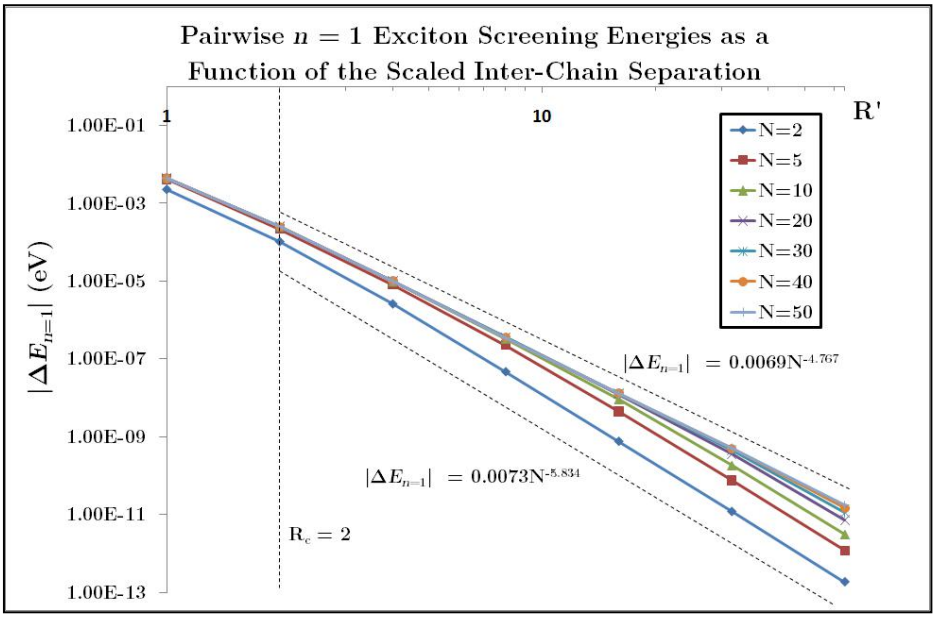

Fig. 4.8: The $n = 1$ exciton dispersion interaction, $|\Delta E_{n=1}|$, between a pair of parallel PPV chains as a function of the scaled inter–chain separation, R'.

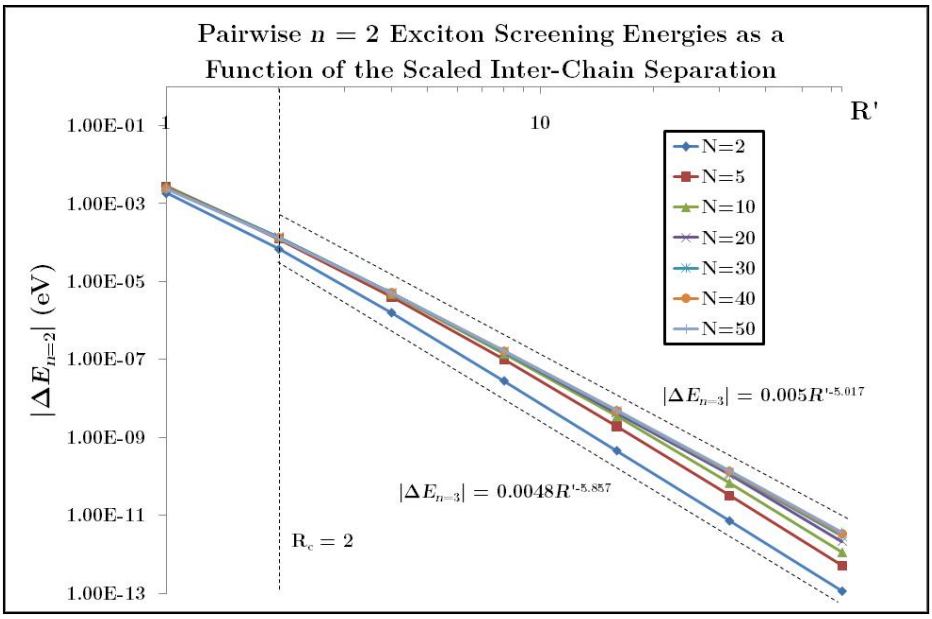

Fig. 4.9: The $n = 2$ exciton dispersion interaction, $|\Delta E_{n=2}|$, between a pair of parallel PPV chains as a function of the scaled inter–chain separation, R'.

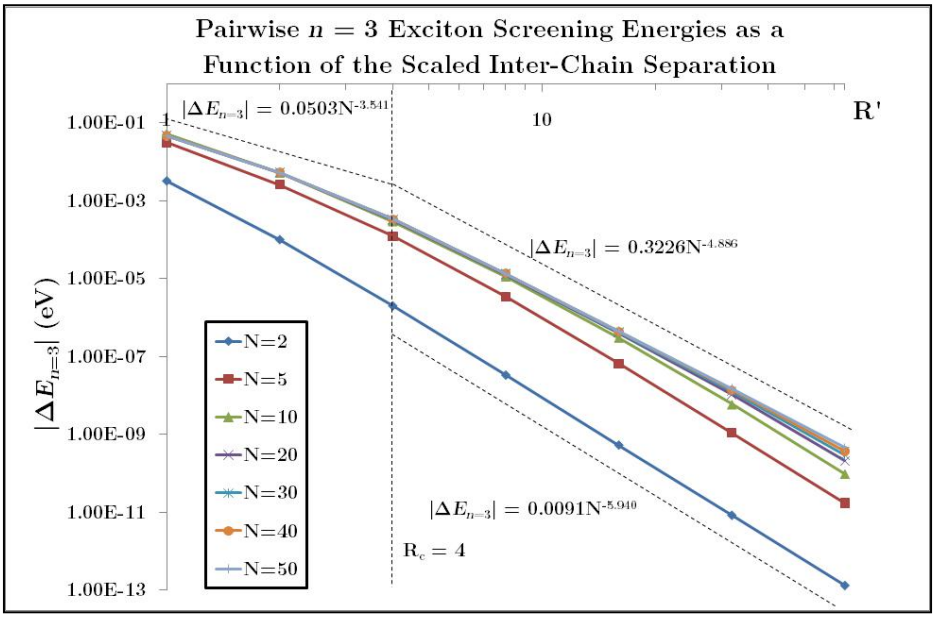

Fig. 4.10: The $n = 3$ exciton dispersion interaction, $|\Delta E_{n=3}|$, between a pair of parallel PPV chains as a function of the scaled inter–chain separation, R'.

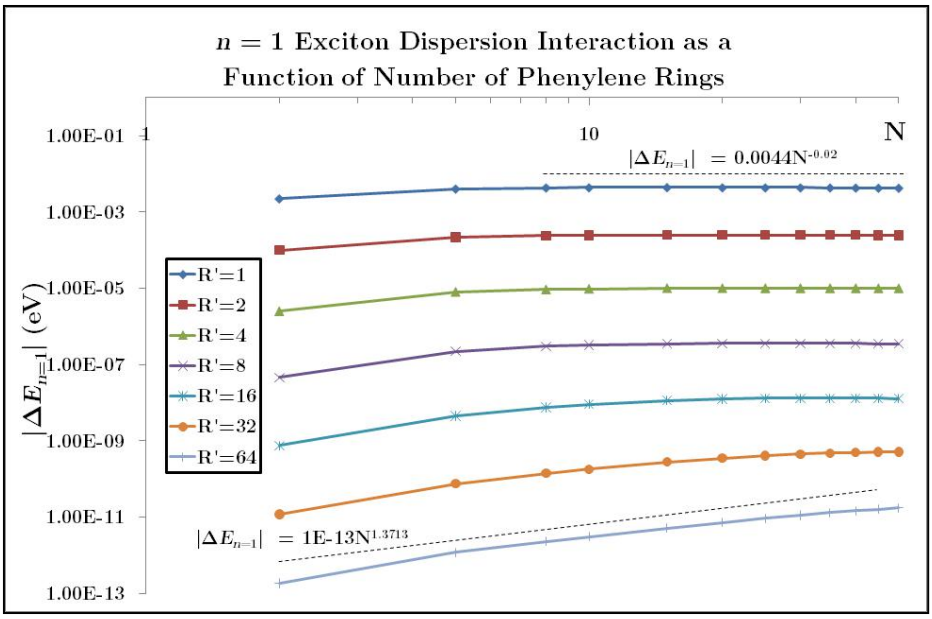

Fig. 4.11: The $n = 1$ exciton dispersion interaction, $|\Delta E_{n=1}|$, between a pair of parallel PPV chains as a function of the number of phenylene rings, N. The results show that for $N \ll R'$, $\Delta E_{GS} \sim N$, while for $N \gg R'$, $\Delta E_{GS} \sim N^0$.

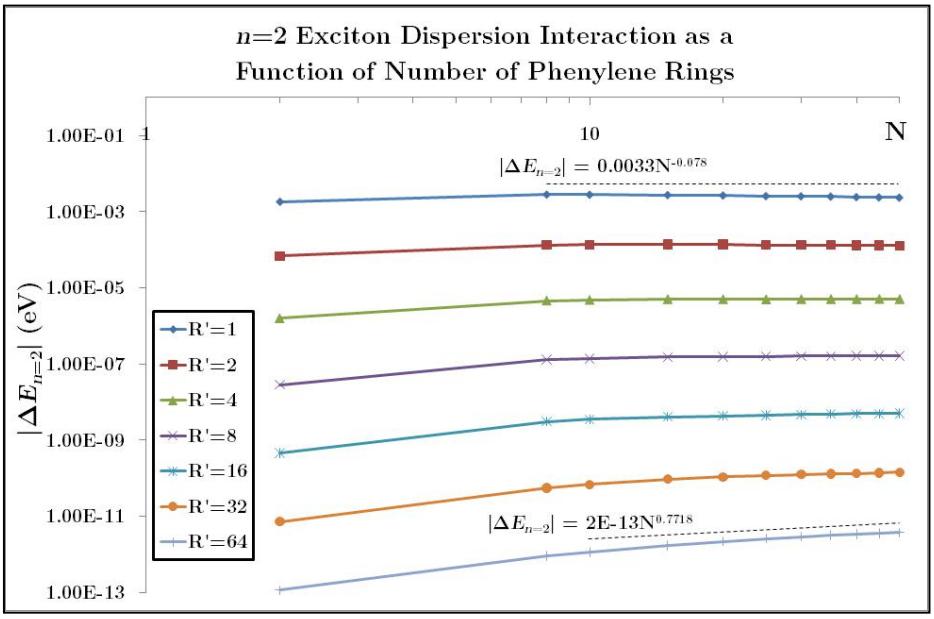

Fig. 4.12: The $n = 2$ exciton dispersion interaction, $|\Delta E_{n=2}|$, between a pair of parallel PPV chains as a function of the number of phenylene rings, N. The results show that for $N \ll R'$, $\Delta E_{GS} \sim N$, while for $N \gg R'$, $\Delta E_{GS} \sim N^0$.

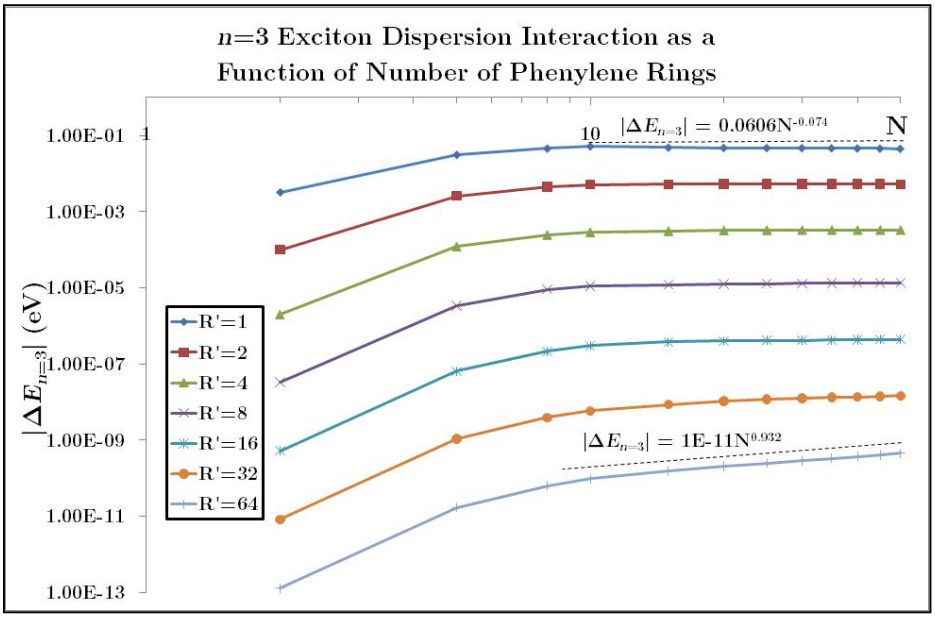

Fig. 4.13: The $n = 3$ dispersion interaction, $|\Delta E_{n=3}|$, between a pair of parallel PPV chains as a function of the number of phenylene rings, N. The results show that for $N \ll R'$, $\Delta E_{GS} \sim N$, while for $N \gg R'$, $\Delta E_{GS} \sim N^0$.

4.4 Lattice Screening

As mentioned in London's seminar paper of 1930, second order dispersion interactions are pair–wise additive. This allows us to make a qualitative prediction for the screening of the excited states in a solid state environment by assuming the crystal structure described in Section 2.4.

The unscreened and lattice–screened excitation energies of the $n = 1$, 2 and 3 excitons for a staggered PPV chain are shown in Fig. 4.15. The lattice spacing was then increased and decreased by 10%. Fig. 4.16 – 4.18 show the screening of the $n = 1 - 3$ exciton energies on separate diagrams.

The following observations can be made:

1) A larger value of the exciton number n corresponds to a larger value of ΔE_n. It is very clear from Fig. 4.14 that the stabilization of the $n = 3$ exciton state is a lot more significant than the $n = 1$ and 2 exciton states.

Their magnitudes relative to the $n = 3$ exciton screening energy go as $\Delta E_{n=3} \backsimeq 2 \times \Delta E_{n=2} \backsimeq 10 \times \Delta E_{n=1}$.

As explained in [16], this occurs due to two main reasons. Firstly, larger n values correspond to larger r_{rms} values as mentioned previously, and therefore larger electron–hole separations. This in turn leads to monopole–dipole interactions dominating dipole–dipole interactions. Second, higher energy exciton states are more effectively solvated by the solid state environment according to first–order time–dependent perturbation theory. If a PPV chain is prepared in a zeroth–order eigenstate $|\Psi_n^{(0)}\rangle$ at time $t = 0$, then the time–dependence of the resulting non–stationary state is described as:

$$|\Psi\rangle(t) = |\Psi_n^{(0)}\rangle + 2 \sum_{n' \neq n} \frac{V_{nn'}}{\Delta E_{nn'}} |\Psi_{n'}^{(0)}\rangle e^{\frac{i\Delta E_{nn'} t}{\hbar}} \qquad (4.4)$$

where $\Delta E_{nn'}$ is the transition energy between $|\Psi_n^{(0)}\rangle$ and the virtual unperturbed states $|\Psi_{n'}^{(0)}\rangle$. The time–energy uncertainty relation tells us that the timescale of this fluctuation scales as $\sim \hbar / \Delta E_{nn'}$.

Since $\Delta E_{nn'}$ decreases with increasing principal quantum number, the fluctuation of the $n = 1$ exciton is the fastest, and slowest for the $n = 3$ exciton. In a very simplified sense, the $n = 3$ exciton's electron–hole pair fluctuates much slower and is thus more effectively screened by the environment, which functions as a dielectric. This is known as the 'solvation–like' limit. The $n = 1$ exciton fluctuation is of the same order as the dielectric, and thus is less effectively solvated. This is referred to as the 'dispersion–like' limit.

2) Compared to the results for polyacetylene [16], the $n = 3$ exciton is not so strongly screened and still lies above the screened energy of the $n = 2$

exciton and the ordering of the screened energy levels still follow the ordering of the n values. In quantitative terms, $\Delta E_{n=1} \simeq 0.04\,e$, $\Delta E_{n=2} \simeq 0.2\,eV$ and $\Delta E_{n=3} \simeq 0.4\,eV$ but these are only qualitatively correct since they depend on the choice of parameters in the Ohno potential.

3) There is a strong dependence of the screening energies on lattice spacing (recall that $\Delta E \sim R^{-v}$, $v \geq 3$). A 10% decrease in the lattice parameters a and b causes a 44%, 49% and 29% increase in the $n = 1$, 2 and 3 exciton screening energies respectively. Similarly, a 10% increase in the lattice parameters causes a 29%, 31% and 22% decrease in the $n = 1$, 2 and 3 exciton screening energies respectively. This would mean that the screening energies depend strongly on density fluctuations.

4) It is clear from Fig. 4.15 that the screened $n = 1$ exciton energy decreases monotonically with increasing N and reaches a constant value of 2.90 eV for a large number of rings. This suggests that the $n = 1$ exciton screening energies decrease roughly at the same rate as the $n = 1$ exciton energies decrease with increasing N and is expected.

5) What is unexpected, however, is that the screened $n = 2$ and 3 exciton energies, do not decrease monotonically with increasing N. The energy curves in Fig. 4.16 amd 4.17 have turning points at approximately $N = 4$ and 7 respectively. This non–monotonic behaviour is clearly not due to a convergence failure, at least, up till second–order perturbation theory — as Fig. 4.18 and 4.19 illustrate, this behaviour persists even when 10 exciton families are included in the sum, and the turning points remain fairly constant with respect to the value of N.

   This might be a non–physical error that arises from the accumulation of errors in the calculation of the transition densities that appear in

equations (2.64) and (2.65). The matrix element V_{FI} in these two equations is a delicate sum of terms that oscillate in sign, as mentioned in Section 4.2.2, and this is illustrated in Fig. 4.15 — the addition of many such transition densities that have small associated errors and oscillate in sign results in an inevitable accumulation of errors.

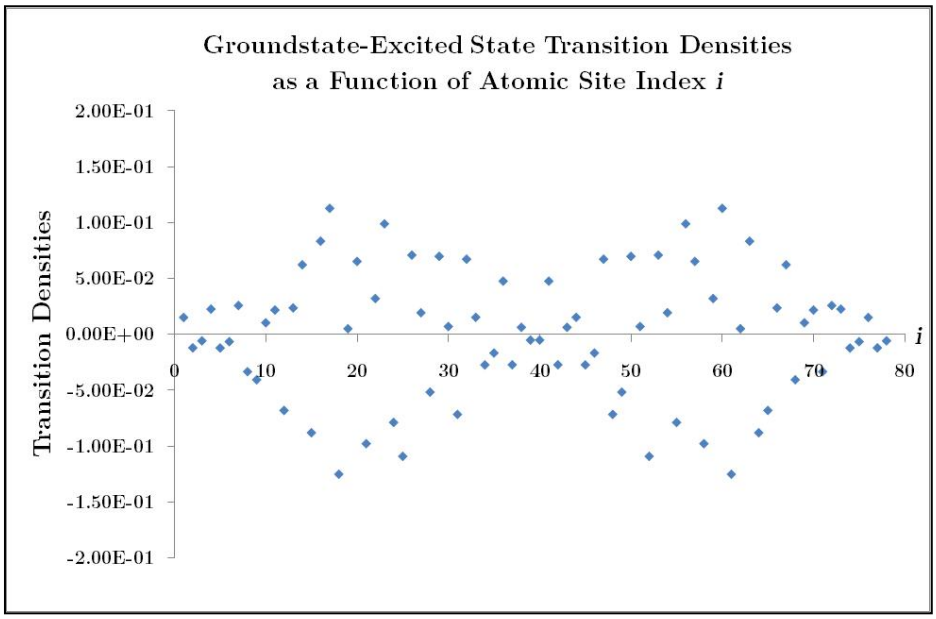

Fig. 4.15: The groundstate–excited state transition densities as a function of atomic site index *i* for a PPV chain with 10 phenylene rings (78 atoms).

For increasingly longer chain lengths with a larger number of atomic indices, the sum of the transition densities might therefore be increasingly less accurate. The higher energy exciton wavefunctions (the $n = 3$ exciton is 75 states above the $n = 1$ exciton for a PPV chain of 50 units) are also less accurate than lower exciton wavefunctions.

Moreover, neglecting the bi–exciton term for the case of PPV chains mentioned in Section 2.4.2 might have more pronounced effects for longer chain lengths than expected as compared to the case of polyacetylene or poly(*p*–phenylene) chains [16] — in this work, notice how the unscreened exciton energies reach a constant value very fast with

respect to the number of phenylene rings N, which means that small errors in the screening energies have a more pronounced effect on the qualitative trend.

There are many other inherent problems such as the use of the Ohno potential, which only models the Coulombic interaction exactly as $r \to \infty$. In this work, perturbation theory was applied up to second–order and thus higher–order terms might be necessary to obtain the correct qualitative trendline. Other methods of calculation are necessary to correct this problem, as outlined in the future work section in the conclusion.

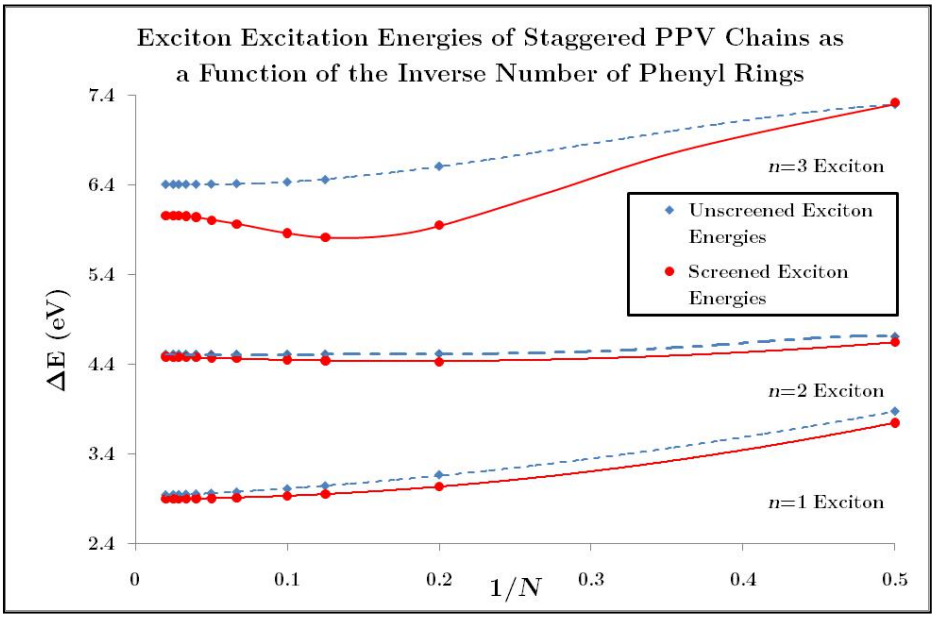

Fig. 4.14: The unscreened and lattice–screened $n = 1 - 3$ exciton energies for a staggered PPV chain as a function of the inverse number of phenyl rings.

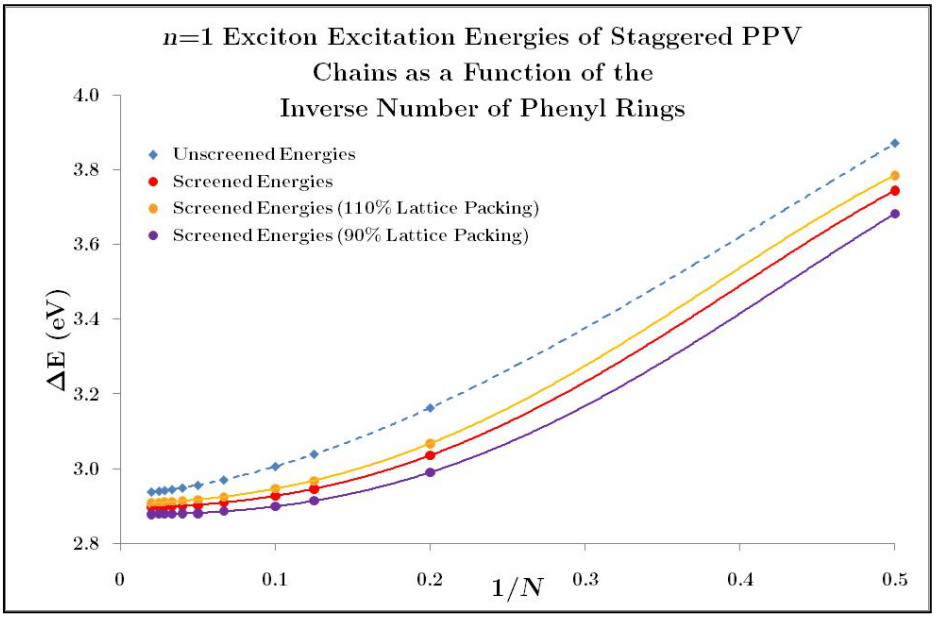

Fig. 4.15: The unscreened and lattice-screened $n = 1$ exciton energies for a staggered PPV chain as a function of the inverse number of phenyl rings. 110% and 90% lattice packing indicates that the lattice spacing was scaled by 110% and 90% respectively.

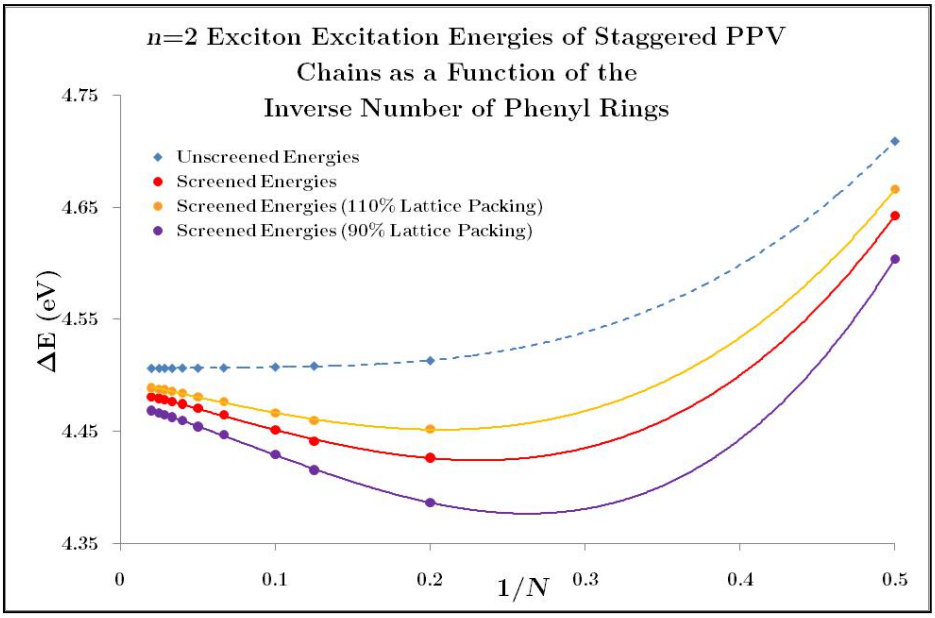

Fig. 4.16: The unscreened and lattice-screened $n = 2$ exciton energies for a staggered PPV chain as a function of the inverse number of phenyl rings. 110% and 90% lattice packing indicates that the lattice spacing was scaled by 110% and 90% respectively.

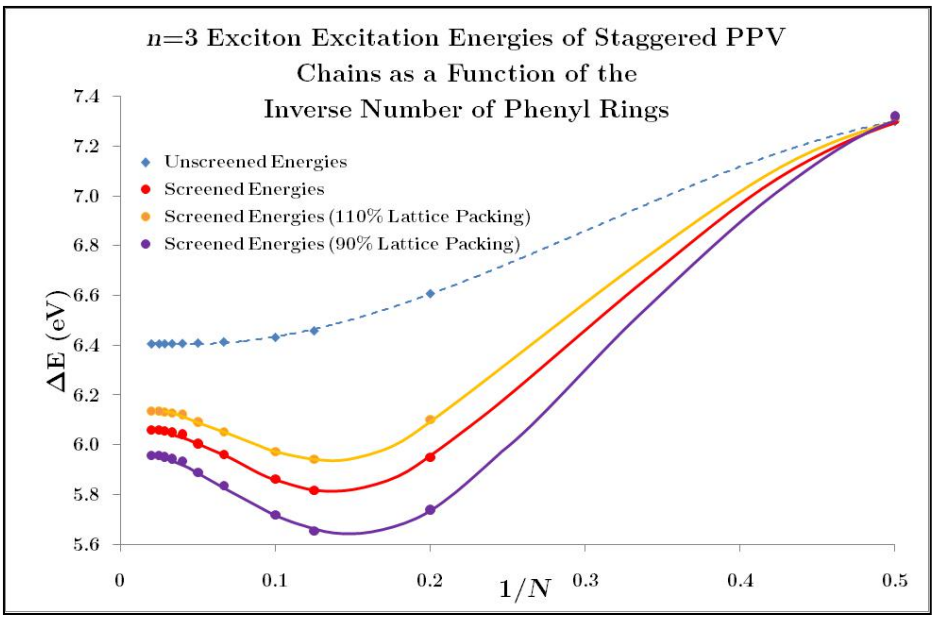

Fig. 4.17: The unscreened and lattice–screened $n = 3$ exciton energies for a staggered PPV chain as a function of the inverse number of phenyl rings. 110% and 90% lattice packing indicates that the lattice spacing was scaled by 110% and 90% respectively.

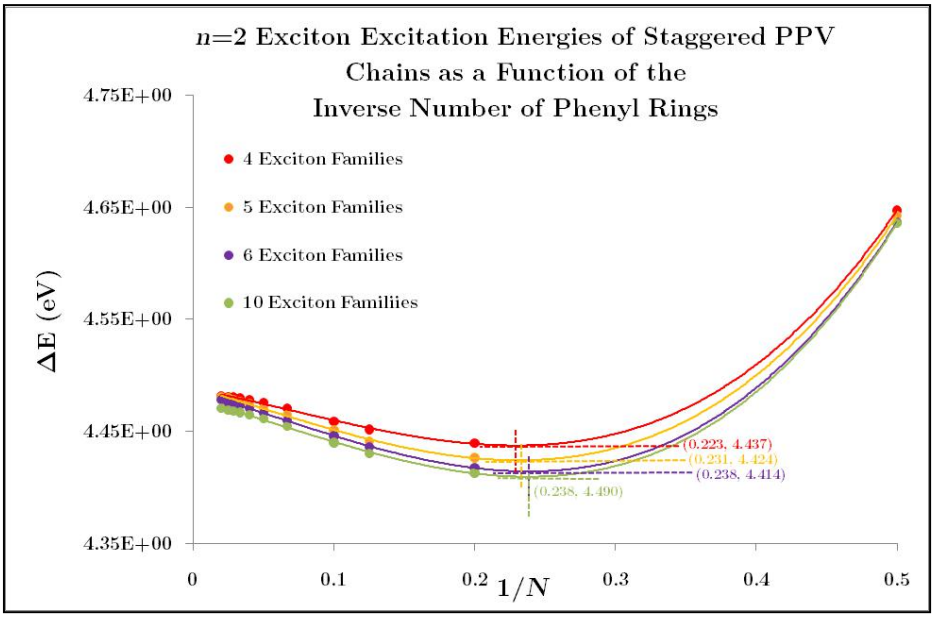

Fig. 4.18: The lattice–screened $n = 2$ exciton energies for a staggered PPV chain as a function of the inverse number of phenyl rings for 4, 5, 6 and 10 exciton families included in the second–order sum.

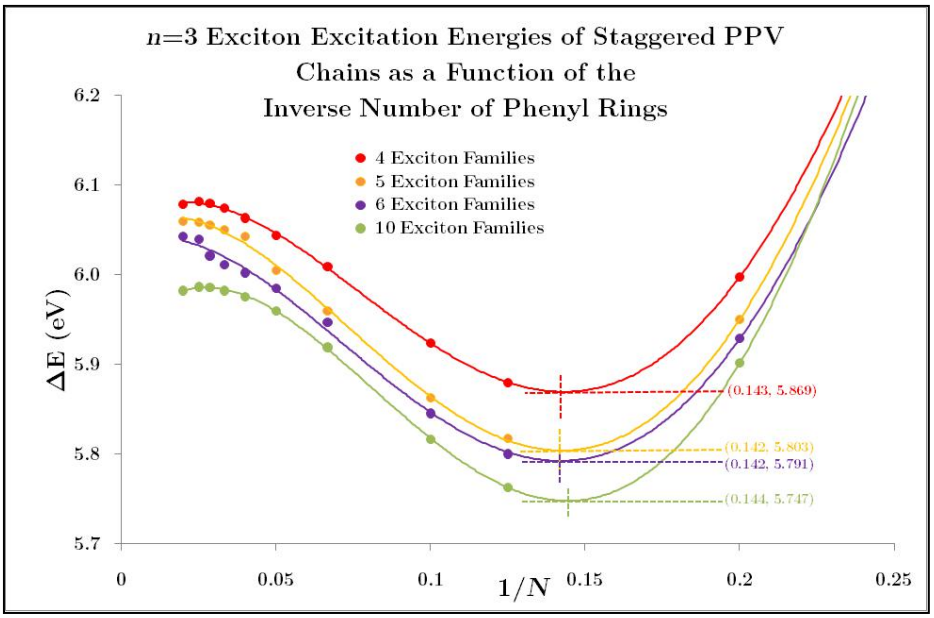

Fig. 4.19: The lattice–screened $n = 3$ exciton energies for a staggered PPV chain as a function of the inverse number of phenyl rings for 4, 5, 6 and 10 exciton families included in the second–order sum.

5 Conclusions

The excited states of a PPV chain were modelled as electron–hole exciton states in terms of the Pariser–Parr–Pople model. While the groundstate was described by the HF method, CI–S theory described the correlation of electrons and provided an exciton basis set of singly–excited determinants to construct the exciton wave functions in the framework of the Mott–Wannier exciton model.

Second–order perturbation theory was used to determine the dispersion interactions between PPV chains. As a compromise between the accuracy of the calculation and the computational time required, all calculations were performed with retention of the first five exciton families in the second–order sum unless otherwise stated.

A summary of the scaling of the groundstate and excited state dispersion energies as a function of the scaled chain separation R' and number of phenylene rings N is given in Table 5.1. All scaling laws are explained within the distributed dipole approximation.

Groundstate		**Excited State**		**Interaction**
Condition	Scaling	Condition	Scaling	**Type**
$N \ll R'$	N^2/R'^6	$R_c < N \ll R'$	N/R'^6	Dipole–Dipole
$N \sim R'$	N/R'^5	$R_c < N \sim R'$	N^0/R'^5	Line Dipole–Line Dipole
償–		$R' < R_c < N$	R'^{-v}, $v \simeq 3$	Monopole–Line Dipole

Table 5.1: Scaling of the groundstate and excited state dispersion interactions as a function of R' and N.

The pair–wise additivity of second order dispersion interactions allowed a qualitative prediction for the screening of the excited states in a solid state environment by assuming the crystal structure described in Section 2.4.

A larger value of the exciton number n corresponds to a larger value of ΔE_n. Their magnitudes relative to the $n = 3$ exciton screening energy go as $\Delta E_{n=3} \simeq 2 \times \Delta E_{n=2} \simeq 10 \times \Delta E_{n=1}$. The ordering of the screened energy levels still follow the ordering of the n values.

There is a strong dependence of the screening energies on lattice spacing. A 10% decrease in the lattice parameters a and b causes a 44%, 49% and 29% increase in the $n = 1$, 2 and 3 exciton screening energies respectively. This would mean that the screening energies depend strongly on density fluctuations.

Future work in this area could possibly give more focus to the following areas:

1) Inclusion of the bi-exciton term mentioned in Section 2.4.2. This would account for the screening interaction between the transition dipole moment of $|\beta'\rangle_2$ with that of $|\alpha'\rangle_1$, which may not be negligible for the exciton screening energies.

2) In this work, the Pariser-Parr-Pople model was used, which did not take into account electron-lattice interactions. It has been shown, however, that such electron-lattice coupling interactions are important — the Su-Schrieffer-Heeger model [34] is a simplified electron-phonon coupling model that may be used to investigate the importance of such interactions in the case of PPV.

3) Accurate calculation of transition densities between excited states is computationally difficult and a simple exciton model might be too crude an approximation. This then limits the reliability of perturbation theory, at least, up till second-order. It might be helpful to consider higher-order perturbation theory or turn towards other methods of calculation, such as the Density Matrix Renormalization Group technique (DMRG) developed by S. R. White [35].

6 Bibliography

1 Burroughes, J. H., Bradley, D. D. C., Brown, A. R. et al. *Nature*, 347 (1990), 539.

2 Bradley, D. D. C. *J. Phys. D: Appl. Phys.*, 20, 11 (1987), 1389.

3 Murase, I., Ohnishi, T., Noguchi, T., and Hirooka, M. *Polym. Commun.*, 25 (1984), 327.

4 Bradley, D. D. C. and Friend, R. H. *J. Phys.: Condensed Matter*, 1 (1989), 3671.

5 Wallace, G. G., Spinks, G. M., Kane–Maguire, L. A. P., and Teasdale, P. R. *Conductive Electroactive Polymers*. CRC Press, 2009.

6 Capistran, J. D., Gagnon, D. R., Antoun, S., Lenz, R. W., and Karasz, F. E. *ACS Polym. Preprints*, 25 (1984), 282.

7 Greiner, A. *Trends Polym. ScL*, 5 (1997), 12.

8 London, F. *Z. Phys. Chem. Abt. B*, 11 (1930), 22.

9 London, F. *Trans. Faraday Soc.*, 33 (1937), 8b.

10 Salem, L. *J. Chem. Phys.*, 37 (1962), 2100.

11 Becke, A. D. and Johnson, E. R. *J. Chem. Phys.*, 122 (2005), 154104.

12 Barford, W. and Xu, X. *J. Chem. Phys.*, 128 (2008), 34705.

13 Pariser, R. and Parr, R. G. *J. Chem. Phys.*, 21, 3 (1953), 466.

14 Barford, W. *J. Chem. Phys.*, 126 (2007), 134905.

15 Beenken, W. J. D. and Pullerits, T. *J. Chem. Phys.*, 120 (2004), 2490.

16 Barford, W., Paiboonvorachat, N., and Yaron, D. *J. Chem. Phys.*, 134 (2011), 234101.

17 Mott, N. *Trans. Faraday Soc.*, 34 (1938), 500.

18 Wannier, G. H. *Phys. Rev.*, 52 (1937), 191.

19 Frenkel, J. *Phys. Rev.*, 37 (1931), 17.

20 Sariciftci, N. S. *Primary Photoexcitations in Conjugated Polymers: Molecular Exciton VS. Semiconductor Band Model*. World Scientific, 1997.

21 Barford, W. *International Series of Monographs on Physics Volume 129: Electronic and Optical Properties of Conjugated Polymers*. Oxford University Press, 2005.

22 Roothaan, C. C. J. *Rev. Mod. Phys.*, 23 (1951), 69.

23 Abrikosov, A. A., Gorkov, L. P., and Dzyloshinski, I. E. *Methods of Quantum Field Theory in Statistical Physics*. Dover Publications, Inc., 1975.

24 Hückel, E. *Zeitschrift für Physik*, 70 (1931), 204.

25 Pariser, R. and Parr, R. G. *J. Chem. Phys.*, 5, 21 (1953), 767.

26 Pople, J. A. *Trans. Faraday Soc.*, 49 (1953), 1375.

27 Oioke, J. A. and Segal, G. A. *J. Chem. Phys.*, 43, 10 (1965), S136.

28 Schrödinger, E. *Annalen der Physik*, 80, 13 (1926), 437.

29 Jeziorski, B., Moszynski, R., and Szalewicz, K. *Chem. Rev.*, 94, 7 (1994), 1887.

30 Chen, D., Winokur, M. J., Masse, M. A., and Karasz, F. E. *Polymer*, 33 (1992), 3117.

31 Wannier, G. H. *Phys. Rev.*, 3, 52 (1937), 191.

32 Claverie, P. and Rein, R. *Int J Quant Chem*, III (1969), 537.

33 Soos, Z. G., Hayden, G. W., McWilliams, P. C. M., and Etemad, S. *J. Chem. Phys.*, 93 (1990), 7439.

34 Su, W–P., Schrieffer, J. R., and Heeger, A. J. *Phys. Rev. Lett.*, 42 (1979), 1698.

35 White, S. R. (1992), 2863.

Appendix A

Self-Consistent Field Procedure

In this Appendix, the Self-Consistent Field (SCF) algorithm will be outlined in the framework of matrix algebra. The Hartree-Fock equation is first written as a matrix equation of the form,

$$\mathbf{FC} = \mathbf{SC}\varepsilon \qquad \text{(A-1)}$$

where **F** is the *Fock matrix* with elements F_{ij},
S is the *overlap matrix* with elements S_{ij},
C is a square matrix with elements C_{im},
ε is a diagonal matrix with elements ε_m.

An orthonormal basis set is used such that **S** is a unit matrix, reducing equation (A-1) to

$$\mathbf{FC} = \mathbf{C}\varepsilon \qquad \text{(A-2)}$$

The algorithm is as follows:

1) Specify a nuclear geometry $\{\mathbf{R}_A\}$, nuclear charge z_A, number of electrons N and a basis set $\{\varphi_i\}$.

2) Calculate and store all integrals required: $(ij|kl)$ and $(i|h|j)$

3) Obtain a guess for the density matrix **P** and its elements P_{ij}.

4) Obtain the Fock matrix **F** from $(i|h|j)$, $(ij|kl)$ and **P**.

5) Diagonalize **F** to obtain **C** and ε.

6) Calculate a new **P** from **C**.

7) Calculate the difference between the new and old **P**: if they are the same, the SCF procedure has achieved convergence; if not, return to step (4).

The total electronic energy of the wave function can then be calculated as

$$E_0 = \frac{1}{2}\sum_{ij} P_{ij}[F_{ij} + (i|h|j)] \qquad \text{(A–3)}$$

Appendix B

Derivation of Transition Densities

In this Appendix, expressions for $\langle GS|N_i|EX|$ and $\langle EX|N_i|EX|$ within a CI–S basis will be derived in a second quantization framework, for use in perturbation theory to calculate the dispersion energies. $|EX|$ refers to an exciton state and $|GS|$ refers to the groundstate. In Hartree–Fock theory, the molecular states $\{|m|\}$ are linear combinations of atomic states $\{|i|\}$:

$$|m| = \sum_i |i|\varphi_{im} \tag{B–1a}$$

$$c^\dagger_{m\sigma} = \sum_i c^\dagger_{i\sigma}\varphi_{im} \tag{B–1b}$$

The reverse unitary transform exists:

$$|i| = \sum_i |m|\varphi^*_{im} \tag{B–1c}$$

$$c^\dagger_{i\sigma} = \sum_i c^\dagger_{m\sigma}\varphi^*_{im} \tag{B–1d}$$

The number operator for the number of electrons in atomic orbital i may be expressed in the molecular orbital basis, in the second quantization framework:

$$N_i = \sum_\sigma c^\dagger_{i\sigma}c_{i\sigma} = \sum_\sigma \sum_{m,n} \varphi^*_{im}\varphi_{in}c^\dagger_{m\sigma}c_{n\sigma} \tag{B–2}$$

Suppose we work with singlet configurations: the excited state $|EX|$ is simply a linear combination of singly–excited singlet spin–adapted determinants $|{}^1\Psi^r_a|$, which we can construct from the HF ground state $|\Psi_0|$:

$$|EX| = \sum_{a,r} \psi^r_a |{}^1\Psi^r_a| = \frac{1}{\sqrt{2}}\sum_\sigma \sum_{a,r} \psi^r_a c^\dagger_{r\sigma}c_{a\sigma}|\Psi_0| \tag{B–3}$$

where $\{a\}$ and $\{r\}$ are the set of occupied and virtual MO indices respectively.

Derivation of $\langle GS|N_i|EX|$

The 1st matrix element follows rather simply:

$$\langle GS|N_i|EX| = \frac{1}{\sqrt{2}} \sum_{\sigma,\sigma'} \sum_{m,n} \sum_{a,r} \varphi^*_{im} \varphi_{in} \psi^r_a \langle \Psi_0 | c^\dagger_{m\sigma'} c_{n\sigma'} c^\dagger_{r\sigma} c_{a\sigma} | \Psi_0 | \qquad \text{(B–4)}$$

Exchanging $c_{a\sigma}$ and $c^\dagger_{r\sigma}$ pair–wise towards the left using the anti–commutation relations:

$$\begin{aligned}
&\langle \Psi_0 | c^\dagger_{m\sigma'} c_{n\sigma'} c^\dagger_{r\sigma} c_{a\sigma} | \Psi_0 | \\
&= \delta_{nr} \delta_{\sigma\sigma'} \langle \Psi_0 | c^\dagger_{m\sigma'} c_{a\sigma} | \Psi_0 | - \langle \Psi_0 | c^\dagger_{m\sigma'} c^\dagger_{r\sigma} c_{n\sigma'} c_{a\sigma} | \Psi_0 | \\
&= \delta_{nr} \delta_{am} \delta_{\sigma\sigma'} \langle \Psi_0 | \Psi_0 | - \delta_{nr} \delta_{\sigma\sigma'} \langle \Psi_0 | c_{a\sigma} c^\dagger_{m\sigma'} | \Psi_0 | + \langle \Psi_0 | c^\dagger_{r\sigma} c^\dagger_{m\sigma'} c_{n\sigma'} c_{a\sigma} | \Psi_0 |
\end{aligned}$$

The last two terms vanish because of $\langle \Psi_0 / c_{a\sigma} = \langle \Psi_0 / c^\dagger_{r\sigma} = 0$ and the first term is simplified to a product of kronecker deltas if one uses a normalized ground state vector:

$$\langle \Psi_0 | c^\dagger_{m\sigma'} c_{n\sigma'} c^\dagger_{r\sigma} c_{a\sigma} | \Psi_0 | = \delta_{nr} \delta_{am} \delta_{\sigma\sigma'} \qquad \text{(B–5)}$$

And so we have, summing over both spin up and down indices,

$$\begin{aligned}
\langle GS|N_i|EX| &= \frac{1}{\sqrt{2}} \sum_{\sigma} \sum_{a,r} \varphi^*_{ia} \varphi_{ir} \psi^r_a \\
&= \sqrt{2} \sum_{a,r} \varphi^*_{ia} \varphi_{ir} \psi^r_a
\end{aligned} \qquad \text{(B–6)}$$

Derivation of $\langle EX|N_i|EX'|$

The 2nd matrix element is derived similarly,

$$\begin{aligned}
\langle EX|N_i|EX'| = \frac{1}{2} &\sum_{\sigma,\sigma',\sigma^*} \sum_{a,r} \sum_{b,s} \sum_{m,n} \chi^{*s}_b \psi^r_a \phi^*_{im} \phi_{in} \\
&\times \langle \Psi_0 | c^\dagger_{b\sigma^*} c_{s\sigma^*} c^\dagger_{m\sigma'} c_{n\sigma'} c^\dagger_{r\sigma} c_{a\sigma} | \Psi_0 |
\end{aligned} \qquad \text{(B–7)}$$

Exchanging $c_{a\sigma}$ and $c^{\dagger}_{r\sigma}$ pair–wise towards the left, $c^{\dagger}_{b\sigma^*}$ and $c_{s\sigma^*}$ towards the right using the anti–commutation relations:

$$\begin{aligned}
&\langle\Psi_0|c^{\dagger}_{b\sigma^*}c_{s\sigma^*}c^{\dagger}_{m\sigma'}c_{n\sigma'}c^{\dagger}_{r\sigma}c_{a\sigma}|\Psi_0| \\
&= \delta_{nr}\delta_{\sigma\sigma'}\langle\Psi_0|c^{\dagger}_{b\sigma^*}c_{s\sigma^*}c^{\dagger}_{m\sigma'}c_{a\sigma}|\Psi_0| \quad \langle\Psi_0|c^{\dagger}_{b\sigma^*}c_{s\sigma^*}c^{\dagger}_{m\sigma'}c^{\dagger}_{r\sigma}c_{n\sigma'}c_{a\sigma}|\Psi_0| \\
&= \delta_{nr}\delta_{am}\delta_{\sigma\sigma'}\langle\Psi_0|c^{\dagger}_{b\sigma^*}c_{s\sigma^*}|\Psi_0| \quad \delta_{nr}\delta_{\sigma\sigma'}\langle\Psi_0|c^{\dagger}_{b\sigma^*}c_{s\sigma^*}c_{a\sigma}c^{\dagger}_{m\sigma'}|\Psi_0| \\
&\quad -\langle\Psi_0|c^{\dagger}_{b\sigma^*}c_{s\sigma^*}c^{\dagger}_{m\sigma'}c^{\dagger}_{r\sigma}c_{n\sigma'}c_{a\sigma}|\Psi_0|
\end{aligned}$$

Because $c_{s\sigma^*}|\Psi_0| = 0$, the first term vanishes; the second term is easily reduced:

$$\begin{aligned}
&\delta_{nr}\delta_{\sigma\sigma'}\langle\Psi_0|c^{\dagger}_{b\sigma^*}c_{s\sigma^*}c_{a\sigma}c^{\dagger}_{m\sigma'}|\Psi_0| \\
&= \delta_{nr}\delta_{\sigma\sigma'}\langle\Psi_0|c^{\dagger}_{b\sigma^*}c_{a\sigma}c_{s\sigma^*}c^{\dagger}_{m\sigma'}|\Psi_0| \\
&= \delta_{nr}\delta_{ab}\delta_{\sigma\sigma'}\delta_{\sigma\sigma^*}\langle\Psi_0|c_{s\sigma^*}c^{\dagger}_{m\sigma'}|\Psi_0| \quad \delta_{nr}\langle\Psi_0|c_{a\sigma}c^{\dagger}_{b\sigma^*}c_{s\sigma^*}c^{\dagger}_{m\sigma'}|\Psi_0| \\
&= \delta_{nr}\delta_{ab}\delta_{sm}\delta_{\sigma\sigma'}\delta_{\sigma\sigma^*}\delta_{\sigma'\sigma^*} \quad \delta_{nr}\delta_{ab}\delta_{\sigma\sigma'}\delta_{\sigma\sigma^*}\langle\Psi_0|c^{\dagger}_{m\sigma'}c_{s\sigma^*}|\Psi_0| \\
&\quad -\delta_{nr}\langle\Psi_0|c_{a\sigma}c^{\dagger}_{b\sigma^*}c_{s\sigma^*}c^{\dagger}_{m\sigma'}|\Psi_0|
\end{aligned}$$

Because $\langle\Psi_0|c_{a\sigma} = c_{s\sigma^*}|\Psi_0| = 0$, the second and third terms vanish:

$$\delta_{nr}\delta_{\sigma\sigma'}\langle\Psi_0|c^{\dagger}_{b\sigma^*}c_{s\sigma^*}c_{a\sigma}c^{\dagger}_{m\sigma'}|\Psi_0| = \delta_{nr}\delta_{ab}\delta_{sm}\delta_{\sigma\sigma'}\delta_{\sigma\sigma^*}\delta_{\sigma'\sigma^*} \qquad \text{(B–8)}$$

This leaves us only with the term $\langle\Psi_0|c^{\dagger}_{b\sigma^*}c_{s\sigma^*}c^{\dagger}_{m\sigma'}c^{\dagger}_{r\sigma}c_{n\sigma'}c_{a\sigma}|\Psi_0|$ to simplify:

$$\begin{aligned}
&\langle\Psi_0|c^{\dagger}_{b\sigma^*}c_{s\sigma^*}c^{\dagger}_{m\sigma'}c^{\dagger}_{r\sigma}c_{n\sigma'}c_{a\sigma}|\Psi_0| \\
&= \langle\Psi_0|c^{\dagger}_{b\sigma^*}c_{s\sigma^*}c^{\dagger}_{r\sigma}c^{\dagger}_{m\sigma'}c_{n\sigma'}c_{a\sigma}|\Psi_0| \\
&= \delta_{rs}\delta_{\sigma\sigma^*}\langle\Psi_0|c^{\dagger}_{b\sigma^*}c^{\dagger}_{m\sigma'}c_{n\sigma'}c_{a\sigma}|\Psi_0| \quad \langle\Psi_0|c^{\dagger}_{b\sigma^*}c^{\dagger}_{r\sigma}c_{s\sigma^*}c^{\dagger}_{m\sigma'}c_{n\sigma'}c_{a\sigma}|\Psi_0| \\
&= \delta_{rs}\delta_{\sigma\sigma^*}\langle\Psi_0|c^{\dagger}_{m\sigma'}c^{\dagger}_{b\sigma^*}c_{n\sigma'}c_{a\sigma}|\Psi_0| + \langle\Psi_0|c^{\dagger}_{r\sigma}c^{\dagger}_{b\sigma^*}c_{s\sigma^*}c^{\dagger}_{m\sigma'}c_{n\sigma'}c_{a\sigma}|\Psi_0|
\end{aligned}$$

Since $\langle\Psi_0|c^{\dagger}_{r\sigma} = 0$, the second term vanishes, leaving us with:

$$
\begin{aligned}
&\langle\Psi_0|c^{\dagger}_{b\sigma^*}c_{s\sigma^*}c^{\dagger}_{m\sigma'}c^{\dagger}_{r\sigma}c_{n\sigma'}c_{a\sigma}|\Psi_0|\\
&=\delta_{rs}\delta_{\sigma\sigma^*}\langle\Psi_0|c^{\dagger}_{m\sigma'}c^{\dagger}_{b\sigma^*}c_{n\sigma'}c_{a\sigma}|\Psi_0|\\
&=\delta_{rs}\delta_{bn}\delta_{\sigma\sigma^*}\langle\Psi_0|c^{\dagger}_{m\sigma'}c_{a\sigma}|\Psi_0| \quad \delta_{rs}\delta_{\sigma\sigma^*}\langle\Psi_0|c^{\dagger}_{m\sigma'}c_{n\sigma'}c^{\dagger}_{b\sigma^*}c_{a\sigma}|\Psi_0|\\
&=\delta_{rs}\delta_{bn}\delta_{am}\delta_{\sigma\sigma^*}\delta_{\sigma\sigma'} \quad \delta_{rs}\delta_{bn}\delta_{\sigma\sigma^*}\langle\Psi_0|c_{a\sigma}c^{\dagger}_{m\sigma'}|\Psi_0|\\
&\quad-\delta_{rs}\delta_{ab}\delta_{\sigma\sigma^*}\langle\Psi_0|c^{\dagger}_{m\sigma'}c_{n\sigma'}|\Psi_0|+\delta_{rs}\delta_{\sigma\sigma^*}\langle\Psi_0|c^{\dagger}_{m\sigma'}c_{n\sigma'}c_{a\sigma}c^{\dagger}_{b\sigma^*}|\Psi_0|
\end{aligned}
$$

Since $\langle\Psi_0/c_{a\sigma}=c^{\dagger}_{b\sigma^*}/\Psi_0|=0$, the second and last terms vanish; and since $\langle\Psi_0|c^{\dagger}_{m\sigma'}c_{n\sigma'}|\Psi_0|=\delta_{mn}$, we now have:

$$
\begin{aligned}
&\langle\Psi_0|c^{\dagger}_b c_s c^{\dagger}_m c^{\dagger}_r c_n c_a|\Psi_0|\\
&=\delta_{rs}\delta_{bn}\delta_{am}\delta_{\sigma\sigma^*}\delta_{\sigma\sigma'} \quad \delta_{rs}\delta_{ab}\delta_{mn}\delta_{\sigma\sigma^*}
\end{aligned}
\tag{B–9}
$$

Putting everything together:

$$
\begin{aligned}
&\langle\Psi_0|c^{\dagger}_b c_s c^{\dagger}_m c_n c^{\dagger}_r c_a|\Psi_0|\\
&=\delta_{nr}\delta_{ab}\delta_{sm}\delta_{\sigma\sigma'}\delta_{\sigma\sigma^*}\delta_{\sigma'\sigma^*}+\delta_{rs}\delta_{bn}\delta_{am}\delta_{\sigma\sigma^*}\delta_{\sigma\sigma'}\\
&\quad-\delta_{rs}\delta_{am}\delta_{mn}\delta_{\sigma\sigma^*}
\end{aligned}
\tag{B–10}
$$

And therefore summing over all spin indices, keeping in mind that $\sum_m|\phi_{im}|^2=\frac{1}{2}$ since m would represent the occupied orbitals only,

$$
\begin{aligned}
&\langle EX|N_i|EX'|\\
&=\frac{1}{2}\sum_{\sigma}\sum_{a,r}\sum_{s}\chi^{*s}_a\psi^r_a\phi^*_{is}\phi_{ir}+\frac{1}{2}\sum_{\sigma}\sum_{a,r}\sum_{b}\chi^{*r}_b\psi^r_a\phi^*_{ia}\phi_{ib}\\
&\quad-\frac{1}{2}\sum_{\sigma,\sigma'}\sum_{a,r}\sum_{m}\chi^{*r}_a\psi^r_a|\phi_{im}|^2\\
&=\sum_{a,r}\sum_{s}\chi^{*s}_a\psi^r_a\phi^*_{is}\phi_{ir}+\sum_{a,r}\sum_{b}\chi^{*r}_b\psi^r_a\phi^*_{ia}\phi_{ib}-\sum_{a,r}\chi^{*r}_a\psi^r_a
\end{aligned}
\tag{B–11}
$$

where

$$
\sum_{a,r}\chi^{*r}_a\psi^r_a=\begin{cases}0 \text{ if } |EX|\neq|EX'|\\ 1 \text{ if } |EX|=|EX'|\end{cases}
\tag{B–12}
$$

Appendix C

Program Codes

The program codes used in this work are found in the CD–ROM that is attached to the back of this thesis. All of the codes are written in Fortran 90.

There are 3 program codes that perform the following the calculations:

GSdisp.f90: This program calculates the pairwise groundstate dispersion energies for a PPV chain. Only two choices are available for the PPV chain geometry: 'linear' and 'trans'. The program prints out the SCF MO energies, the exciton energies and other exciton properties as well.

EXdisp.f90: This program calculates the pairwise excited state dispersion energies for a PPV chain. Only two choices are available for the PPV chain geometry: 'linear' and 'trans'. The program prints out the SCF MO energies, the exciton energies and other exciton properties as well.

EXsum.f90: This program calculates the lattice excited state dispersion energies for a PPV chain. Four choices are available for the PPV chain geometry: 'linear', 'trans', 'spiral' and 'staggered'. The program prints out the SCF MO energies, the exciton energies and other exciton properties as well.